Unscrambling Nonlinear Dynamics in Synthetic Aperture Radar Imagery

KHALID EL-DARYMLI[1], (Member, IEEE), ERIC W. GILL[2], (Senior Member, IEEE), PETER MCGUIRE[2,3], DESMOND POWER[3], (Member, IEEE), AND CECILIA MOLONEY[2], (Member, IEEE)

[1]Northern Radar Inc., St. John's, NF A1B 3E4, Canada
[2]Memorial University of Newfoundland, St. John's, NF A1B 3X5, Canada
[3]C-CORE, St. John's, NF A1C 3X5, Canada

Corresponding author: K. El-Darymli (k.el-darymli@northernradar.com)

ABSTRACT In analyzing single-channel synthetic aperture radar (SAR) imagery, three interrelated questions often arise. First, should one use the detected or the complex-valued image? Second, what is the 'best' statistical model? Finally, what constitutes the 'best' signal processing methods? This paper addresses these questions from the overarching perspective of the generalized central limit theorem, which underpins nonlinear signal processing. A novel procedure for characterizing the nonlinear dynamics in SAR imagery is proposed. To apply the procedure, three complementary 1-D abstractions for a 2-D SAR chip are introduced. Our analysis is demonstrated on real-world datasets from multiple SAR sensors. The nonlinear dynamics are found to be resolution dependent. As the SAR chip is detected, nonlinear effects are found to be obliterated (i.e., for magnitude-detection) or altered (i.e., for power-detection). In the presence of extended targets (i.e., nonlinear scatterers), it is recommended to use the complex-valued chip rather than the detected one. Furthermore, to exploit the intrinsic nonlinear statistics, it is advised to utilize relevant nonlinear signal analysis techniques.

INDEX TERMS Generalized central limit theorem, nonlinear dynamics, SAR, complex-valued signal, resolution theory, extended targets.

I. INTRODUCTION

Although we live in an inherently nonlinear world, conventional signal processing is built on linear system theory. This theory treats deviation from linearity as noise that warrants removal. Much of the original interest in nonlinear phenomena arose from the study of deterministic chaos, and subsequent research has branched into an analysis of nonlinearity in general [1]–[3]. Nonlinear-based research efforts can be broadly classified into two main branches: (1) the development of novel methods that seek to explicitly exploit the nonlinear phenomenon, and (2) the advancement of techniques that permit the harnessing of nonlinear dynamics (i.e., so-called nonlinear artifacts) retained in the signal after application of common linear signal processing methods. This paper, concerned with the second branch, is exclusively aimed at the focused *single-channel* and *complex-valued* synthetic aperture radar (SAR) image outputs from SAR processors.

In SAR and its relatives, such as synthetic aperture sonar (SAS), the signal processor focuses 1-D range profiles into a complex-valued image. The underlying assumption which underpins signal processing theory in general, and its application to SAR imagery in particular, is linearity. Indeed, the SAR image is often implicitly assumed to be linear. The assumption of linearity leads to another implicit assumption, that is second-order circularity (also known as propriety) which implies that the phase in complex-valued SAR imagery is non-informative (see [4] for details). This is a consequence of the conventional resolution theory of point targets [5]. Consequently, most of the interest in analyzing the focused single-channel SAR image has traditionally been based on techniques motivated by linear system theory. As a result,

many such linear techniques are associated with the detected SAR image (i.e., image intensity) while the phase content is entirely ignored [6]. With the advent of high-resolution remote sensors, the insufficiency of this theory as applied to both stationary and moving extended targets has been reported in the literature [7]–[11]. This conclusion is based on the empirical observation that extended targets, such as vehicles and airplanes, produce dispersive scattering from cavity-like reflectors. In effect, this induces a nonlinear phase modulation in the radar return signal which causes a mismatch in the correlator's output. This phenomenon is referred to as 'sideband responses', and much of the information about it is preserved in the complex-valued image rather than the detected one.

In the signal processing literature, there are two definitions of linearity considered [12]–[17]: one is the definition of a strictly linear signal, and the other is the commonly adopted definition of a linear signal. In the former, the signal is assumed to be generated by a linear time invariant (LTI) or a linear space invariant (LSI) system with a white Gaussian noise. The commonly adopted definition differs from the former in that the magnitude distribution is allowed to deviate from the Gaussian distribution. This implies that the strictly defined linear signal is allowed to be characterized by a nonlinear observation function, thereby justifying the use of linear signal processing methods on the latter. The main reason for the popularity of linear signal processing techniques is their rich and well-defined linear system theory and simplicity of implementation. However, if the complex-valued SAR data is proven to be nonlinear, significant gains are to be anticipated from applying relevant nonlinear techniques. This is because the nonlinear methods provide for the exploitation of the nonlinear statistics ignored by the common linear signal processing methods. While the SAR sensor is often modeled in the literature as a linear system [5], this does not guarantee that the focused complex-valued image output from the SAR processor is linear, as explained earlier [7]–[11]. Further, in [4], the statistical significance of second-order noncircularity (also known as impropriety) for the case of extended target is clearly demonstrated. This implies that unlike the common belief about the non-informativeness of the phase, the phase is indeed useful.

Although our discussion here is presented in the context of automatic target recognition in SAR imagery (SAR-ATR), which includes both detection and classification, it is straightforward to generalize this discussion to any relevant context. In the detection stage, popular linear statistical models include the Gaussian, exponential, Rayleigh, Gamma, Weibull, and K distributions, etc. [6], [18]. All these linear models implicitly assume the underlying (superimposed) random variables to have a finite variance. Hence, such models are all motivated by the central limit theorem (CLT). On the contrary, nonlinear statistical models are built on the premises that the underlying random variables possess an infinite variance; thus, such models are justified by the generalized central limit theorem (GCLT).

Examples of nonlinear statistical models include the generalized Gaussian distribution (GGD) [17], the complex GGD [19], the symmetric α-stable ($S\alpha S$) distribution [17], the Gaussian scale mixture (GSM) [20], and the wrapped complex Gaussian scale mixture (WCGSM) [4], etc.

In the classification stage, suitable signal processing methods are often used to extract and/or select useful features from the SAR data. These features are used for classifier training and testing. Feature generation methods can be broadly classified into linear and nonlinear/adaptive which are motivated by the CLT theorem and the GCLT theorem, respectively. Among others, popular linear signal processing methods include the Fourier [21], [22], wavelet [23], and Radon transforms [23], [24], and principal component analysis (PCA) [25], while nonlinear signal processing methods similarity include the Hilbert-Huang transform (HHT) [26], nonlinear independent component analysis (nICA) [27], and the weighted myriad filter (WMF) [17]. While many linear signal processing methods are designed to preserve the nonlinear statistics (i.e., in the linearly transformed signal, when the nonlinear statistics are present in the original signal), features generated solely based on the linear statistics will be blind to the nonlinear dynamics.

Based on the preceding discussion, it is clear that a proper understanding of the inherent nature of the complex-valued SAR data in terms of linearity and nonlinearity will not only allow for an informed choice pertaining to the most suitable statistical models and signal processing methods, but also will provide for the extraction of as much information as possible from the SAR data. The novel contributions presented in this paper may be summarized as follows

- A procedure for empirically demonstrating the inapplicability of the CLT theorem and the applicability of the GCLT theorem to extended targets in SAR imagery, and the interrelationship with the spatial resolution of the SAR sensor (see Sect. II-B and Sect. VII-A),
- A method for linearly transforming the real-valued SAR chip from 2-D to 1-D space (see Sect. IV-B),
- A method for linearly transforming the complex-valued SAR chip, in terms of the bivariate statistics, from 2-D to 1-D space (see Sect. IV-C),
- A method for linearly transforming the complex-valued SAR chip, in terms of the complex-valued statistics, from 2-D to 1-D space (see Sect. IV-D), and
- A procedure for detecting and characterizing the statistical significance of nonlinearity in SAR imagery (see Sect. V).

Throughout this paper, the term *SAR* is used to inclusively imply all other signals that possess similar properties. Moreover, the term *high-resolution* is used to nominally refer to a sensor with a spatial resolution greater than the size of the imaged target (i.e., extended target) [28]. Further, the term *chip* is used to refer to a smaller image, for a particular target or clutter, extracted from a bigger scene. Finally, in the present context the term *non-Gaussian* is used synonymously with *nonlinear*.

The remainder of this paper is organized as follows. In Sect. II, the underlying motivations for this study are presented. In Sect. III, the topic of nonlinearity detection in SAR imagery through resampling and hypothesis testing is approached. In Sect. IV, a procedure for linear transformation of the real-valued, as well as the complex-valued, SAR chip from 2-D to 1-D space is proposed. In Sect. V, a procedure for testing the statistical significance of nonlinearity in SAR imagery is outlined. In Sect. VI, the overall SAR datasets used in this study are introduced. In Sect. VII, results are discussed. Finally, a conclusion appears in Sect. VIII.

II. MOTIVATIONS

A. WHY NONLINEAR SIGNAL PROCESSING?

Nonlinear signal processing offers significant advantages over traditional linear signal processing in applications where the underlying random processes are non-Gaussian in nature and/or when the system acting on the signal of interest is inherently nonlinear [17], [19]. Given that the SAR sensor is often modeled as a linear system [5], the former case is of interest here. It is important to precisely explain what is meant by linearity and nonlinearity. The following definitions are used in the literature to characterize the signal's linearity/nonlinearity [12]–[16].

1) DEFINITION OF STRICTLY LINEAR SIGNAL

A signal generated by a linear time invariant (LTI) or a linear space invariant (LSI) system with a white Gaussian noise.

2) COMMONLY ADOPTED DEFINITION OF LINEAR SIGNAL

Similar to the aforementioned definition but the magnitude distribution is allowed to deviate from the Gaussian distribution. This implies that, the strictly defined linear signal is allowed to be characterized by a nonlinear observation function.

3) DEFINITION OF NONLINEAR SIGNAL

Any signal that does not fulfill the definition of either the strictly linear signal or the commonly adopted definition of linear signal.

While much of the original interest in nonlinear phenomena arose from the study of deterministic chaos, subsequent research has branched into an analysis of nonlinearities generally [1]–[3]. In the remote sensing community, this motivated the development of new techniques that are deliberately designed to excite nonlinear scattering in the imaged object, and to properly harness it using suitable nonlinear signal processing methods [29]. One of the most interesting recent studies on the superiority of nonlinear signal processing for sonar is that reported in [29] and [30]. In that study, it is empirically demonstrated that while conventional linear signal processing is not able to distinguish the targets from the bubble clutter, nonlinear signal processing inspired by dolphin-like sonar pulses can both detect and classify such targets. In [29] and [31], the extension

of this technique allowed the development of a new radar which relies on the excitation of nonlinearities in the imaged scene. Nonlinear signal processing was used to differentiate between linear and nonlinear scatterers, thus, improving the target recognition performance of the radar.

B. CENTRAL LIMIT THEOREM (CLT), GENERALIZED CENTRAL LIMIT THEOREM (GCLT), AND SAR IMAGERY

It is intuitive to approach the abovementioned definitions of linearity and nonlinearity from the perspective of the CLT and the GCLT theorems, respectively. In Cases (Sect. II-A1) and (Sect. II-A2) above, the signal is assumed to be linear. For the two cases, this implies that the superposition principle (i.e., additivity and homogeneity) either *strictly* or *approximately* hold, respectively [21], [22], [32]. This is a consequence of the CLT theorem. The classical CLT theorem states that the properly normed sum of a set of independent and identically distributed (iid) random variables, *each with a finite variance*, will tend to Gaussian as the number of variables increases [33]. In Case (Sect. II-A1), the CLT is *strictly* applicable which means that the statistical distribution of the signal can be strictly modeled as Gaussian. However, in many real-world systems the assumption of the strict Gaussianity is impractical. In Case (Sect. II-A2), although a distribution other than (strict) Gaussian can be used to model the (power or magnitude-detected) signal, the applicability of the CLT theorem is still assumed. This is because such distributions (e.g., exponential, Rayleigh, Weibull, etc. [18]), implicitly assume that the random variables they model possess a finite variance. This implies that they lie in the *domain-of-attraction* of the Gaussian distribution (i.e., are asymptotically Gaussian). It transpires that this is the case for any statistical distribution that employs the assumption of finite variance in the random variables modeled. Here, we demonstrate the applicability of this idea to SAR imagery.

In order for Case (Sect. II-A1) to be applicable to SAR imagery, it is required that the complex-valued speckle (i.e., $Y = Y_I + jY_Q$; imaginary unit $j = \sqrt{-1}$, subscripts I and Q denote the real and imaginary parts, respectively), which is modeled as a multiplicative noise, be bivariate Gaussian (i.e., Y_I is strictly Gaussian and Y_Q is strictly Gaussian). Assuming a homogeneous clutter and a single-look SAR processing, the complex-valued backscatter X is constant (i.e., C). Thus, the statistical multiplicative model of the complex-valued SAR image including speckle (i.e., $Z = X\,Y = Z_I + jZ_Q$) is bivariate Gaussian (i.e., $Z = C\,(Y_I + jY_Q)$). This implies that the power-detected SAR image (i.e., $Z_P = Z_I^2 + Z_Q^2$) is exponentially distributed. Further, the magnitude-detected SAR image (i.e., $Z_M = \sqrt{Z_I^2 + Z_Q^2}$) follows Rayleigh distribution. Hence, the phase image follows a uniform distribution. This makes the assumption of linearity strictly applicable. For Case (Sect. II-A2), the assumption that the distribution of the complex-valued Y strictly abides by the bivariate Gaussian is replaced with the properties that Y follows the

Gamma distribution and the square-root Gamma distribution, respectively, in the power-domain and the magnitude-domain. It may be noted that the exponential distribution, mentioned earlier under Case (Sect. II-A1), is a special case of the Gamma distribution. Further, the assumption of constant X is replaced with a particular statistical model in the power or the magnitude domain but not in the complex-valued domain. For example, one of the generic distributions used for modeling the SAR image in the magnitude-domain is the G-distribution. The G-distribution uses the square-root of the generalized inverse Gaussian distribution to model $X_M = \sqrt{X_I^2 + X_Q^2}$ for both homogeneous and heterogeneous backgrounds. The speckle model in the power or the magnitude domain, still follows the Gamma distribution and the square-root Gamma distribution, respectively. Some other popular statistical distributions such as the G^o-distribution and the K-distribution are special cases of the G-distribution. This shows the scope of Case (Sect. II-A2) in the context of SAR imagery. It is clear that in all these cases the distribution of the power-detected or the magnitude-detected SAR image is allowed to deviate from the Gaussian distribution, in order for the non-strict assumption of linearity to hold. It is interesting to note that the implicit assumption here is that all these distributions are in the domain-of-attraction of the Gaussian distribution. Further, in all such statistical models, the complex-valued statistics are entirely ignored due to the assumption that the phase follows a uniform distribution. A detailed explanation on the interrelation between these statistical models for SAR imagery is found in [18, Sec. 5.2].

In Case (Sect. II-A3), due to the *infinite variance* of the signal's distribution (i.e., when the signal is sampled from a population with an infinite variance), the CLT cannot hold. Thus, the CLT is replaced with the Generalized CLT (GCLT). In the GCLT, the Gaussian distribution as a *domain-of-attraction* is replaced with the so-called *stable distribution*. The GCLT states that a sum of independent random variables from the same distribution, when properly centered and scaled, belongs to the domain-of-attraction of a stable distribution. Further, the only distributions that arise as limits from suitably scaled and centered sums of random variables are the stable distributions [17], [34]. Of interest in nonlinear signal processing are the stable Paretian distributions which are strictly non-Gaussian. Note that statistical distributions motivated by the CLT theorem can be viewed as a special case of the GCLT theorem.

Case (Sect. II-A3) motivates the whole research on nonlinear signal processing. The reasoning here is that if one forces a signal sampled from a population which possesses an infinite variance to be modeled, or more generally processed, using a linear technique, one simply ignores some valuable information which can only be exploited through utilizing nonlinear signal processing methods [17]. A practical example is the statistical model often used in the front-end stage (i.e., target detection) of an automatic target recognition (ATR) system. Other examples are the features generated from the target chips for training and testing the intermediate (i.e., low-level classifier) and the back-end (i.e., high-level classifier) stages of the ATR system. The empirical applicability of Case (Sect. II-A3) to high-resolution SAR imagery is discussed in detail in Sect. VII-A.

C. ON THE ORIGIN OF THE NONLINEAR PHENOMENON IN SAR IMAGERY

The baseband backscatter x_{BB} from a single point target, output from the quadrature demodulator and downlinked to the SAR processor, is known as the phase history or the raw signal given by [5]

$$
\begin{aligned}
x_{BB}\left(\underline{\tau}, \eta\right) &= A \exp\left(j\psi\right) \\
&\times \left\{ w_r\left(\underline{\tau} - 2\frac{R(\eta)}{c}\right) w_a\left(\eta - \eta_c\right) \exp \right. \\
&\left. \left(-j4\pi f_o \frac{R(\eta)}{c}\right) \exp\left(j\pi K_r\left(\underline{\tau} - 2\frac{R(\eta)}{c}\right)^2\right) \right\},
\end{aligned}
\tag{1}
$$

where A is the backscatter coefficient (i.e., σ_o), ψ is a phase change in the received pulse due to the scattering process from a surface, $\underline{\tau}$ is the fast time, η is the slow time, $w_r(\underline{\tau}) = rect(\underline{\tau}/T_r)$ is the transmitted pulse envelope, T_r is the pulse duration, $R(\eta)$ is the distance between the radar and the point target, c is the speed of light in a vacuum, $w_a(\eta)$ is the two-way azimuth beam pattern, η_c is the beam center in the azimuth direction, f_o is the center frequency, and K_r is the frequency modulation (FM) rate of the range pulse. The SAR raw signal is conventionally modeled as

$$
x_{BB}\left(\underline{\tau}, \eta\right) = g\left(\underline{\tau}, \eta\right) \otimes h\left(\underline{\tau}, \eta\right) + n\left(\underline{\tau}, \eta\right),
\tag{2}
$$

where $\otimes$ denotes convolution, $g\left(\underline{\tau}, \eta\right)$ is the ground reflectivity, $h\left(\underline{\tau}, \eta\right)$ is the impulse response of the SAR, and $n\left(\underline{\tau}, \eta\right)$ is a noise component mainly due to the front-end receiver.

The SAR processor solves for $g\left(\underline{\tau}, \eta\right)$. Following the conventional radar resolution theory, $h\left(\underline{\tau}, \eta\right)$, bounded by the curly brackets in Eq. 1, is an impulse response of a point target. For a given reflector within the radar illumination time, ψ is assumed to be constant [5]. For the case of an extended target, this assumption is retained. Hence, such a target is modeled as the linear combination of its point reflectors. However, the assumption of constant ψ is violated in the presence of dispersive scattering from cavity-like reflectors, typical in stationary and moving man-made (extended) targets such as vehicles and airplanes. These reflectors trap the incident wave before it is backscattered, thus, inducing a phase modulation (PM). The problem arises when the PM is nonlinear. Besides the PM, this phenomenon also introduces amplitude modulation (AM) [7]–[10]. Thus, the backscatter term in Eq. 1 is rewritten as

$$
s\left(\underline{\tau}(f_\tau), \eta\right) = A\left(\underline{\tau}(f_\tau), \eta\right) \exp\left(j\psi\left(\underline{\tau}(f_\tau), \eta\right)\right),
\tag{3}
$$

where $\underline{\tau}\,(f_\tau)$ is the time delay due to the PM, and f_τ varies over the spectral width of the chirp, B. In Eq. 3, it is emphasized that the magnitude and phase of the backscatter is frequency dependent. While AM is a linear process, this is often not the case for PM. Indeed, based on the principle of stationary phase (POSP), the time delay induced by a dispersive scatterer is

$$\underline{\tau}\,(f_\tau) \propto \frac{d}{df}\,(f_\tau)^O, \tag{4}$$

where O is the order induced by the dispersive scatterer. For $O \in \{0, 1, 2\}$, the PM is linear, and its effect is either translation or smearing of the response in the correlation filter.[1] However, for $O \notin \{0, 1, 2\}$, the phase center possesses a nonlinear delay which introduces spurious effects in the correlator's output. This phenomenon is referred to as 'sideband response', and the information about it is preserved in the complex-valued image rather than the detected one. Further, in the presence of an extended target, it is empirically observed that this effect dominates the focused SAR imagery [7]–[10]. The sideband responses are radically different from the range and Doppler sidelobes. One of the reasons for this is that they are among the strongest responses. Secondly, unlike the range and the Doppler sidelobes, they are not restricted to the range and cross-range gates. Thirdly, they are distributed over an area far larger than that occupied by the target. As stressed in [7]–[9], these sideband responses cannot be suppressed by the weighting methods because they are target generated. It is clear, as a result of the effect, the nonlinear PM violates the resolution theory of point targets.

III. NONLINEARITY DETECTION IN SAR IMAGERY
A. TESTING FOR NONLINEARITY THROUGH RESAMPLING
The most common method for nonlinearity detection in a 1-D signal is that based on the so-called surrogate data test. In this method, a surrogate signal $\{z_t\}_{t=1}^n$ is resampled from an original signal $\{x_t\}_{t=1}^n$ to be tested. The resampled signal should fulfill the following two conditions: (1) it should preserve the linear correlation of the original signal, and (2) it should retain the marginal distribution pertinent to the original signal [35]–[37]. Thus, $\{x_t\}_{t=1}^n$ is resampled in accordance with a null hypothesis $\mathcal{H}_0$ (for linearity) such that a surrogate signal $\{z_t\}_{t=1}^n$ is generated as follows

$$\mathcal{H}_0: z_t = \underline{h}\,(s_t), \quad \{s_t\} \sim \mathcal{N}\,(0, 1, \rho_s), \tag{5}$$

where $\mathcal{H}_0$ is a stochastic linear process, $\{s_t\}$ is a standard Gaussian process, ρ_s is the autocorrelation of s_t, and $\underline{h}$ is a static instantaneous transform which can be linear/nonlinear/monotonic/nonmonotonic. Note that $\mathcal{N}\,(0, 1, \rho_s)$ accounts for the linear dynamics in the input signal and $\underline{h}$ allows for deviations from the marginal Gaussian distribution. Various relevant resampling methods are reported in the literature. Of interest to this study is

[1]Note that smearing also occurs due to the variable Doppler processing used for motion compensation.

the iterative amplitude adjusted Fourier transform (iAAFT) method [38], [39], which is chosen mainly because it is found to give acceptable results [40]. The iAAFT method approximates the sample power spectrum, $S_z(f) \approx S_x(f)$, where $S_x(f)$ is the periodogram of $\{x_t\}_{t=1}^n$. Further, the iAAFT follows the constrained realization approach in a direct attempt to generate surrogate data that fulfill the abovementioned two conditions. Hence, the iAAFT is designed to be used for testing $\mathcal{H}_0$ of a Gaussian process undergoing a static transform (i.e., not only the monotonic, Case (Sect. II-A2) as discussed earlier). The iAAFT surrogate approximates the original autocorrelation (i.e., linear correlation) and possesses the exact original marginal distribution of the input signal [38], [40], [41].

B. MEASURES FOR LINEARITY AND NONLINEARITY
In this study, two kinds of correlation measures are used to account for the linear and nonlinear statistics, respectively. Firstly, for capturing the linear correlation statistics in the SAR chip, we use the Pearson product-moment correlation (PPMC) given in [39] and [42] as

$$r\,(\tau) = \frac{\sum_{t=1}^{n-\tau}(y_t - \bar{y})(y_{t+\tau} - \bar{y})}{\sum_{t=1}^{n-\tau}(y_t - \bar{y})^2}, \tag{6}$$

where τ is a lag and $\bar{y}$ is the mean of $\{y_t\}_{t=1}^n$. Secondly, for capturing the nonlinear correlation statistics, we use the mutual information (MI) defined as [43]

$$
\begin{aligned}
I\,(\tau) = I\,(Y_t, Y_{t-\tau}) = &\sum_{Y_t}\sum_{Y_{t+\tau}} p_{Y_t Y_{t-\tau}}\,(y_t, y_{t-\tau}) \\
&\times \log \frac{p_{Y_t Y_{t-\tau}}\,(y_t, y_{t-\tau})}{p_{Y_t}\,(y_t)\,p_{Y_{t-\tau}}\,(y_{t-\tau})},
\end{aligned} \tag{7}
$$

where $p_{Y_t Y_{t-\tau}}\,(y_t, y_{t-\tau})$ is the joint probability mass function (PMF), and $p_{Y_t}\,(y_t)$ and $p_{Y_{t-\tau}}\,(y_{t-\tau})$ are the marginal PMFs for y_t and $y_{t-\tau}$, respectively. MI is known to be a powerful test statistic for nonlinearity, accounting for both linear and nonlinear behaviors [44]–[46]. To estimate the joint and marginal PMFs of Eq. 7 we use the equiprobable bin histogram (EBH) procedure which partitions the domain of Y_t and $Y_{t-\tau}$ into b intervals of similar occupancy and different width [44], [47], [48]. The histogram bins are chosen to have equal probability rather than equal width as is the usual case. Thus, the width of the bins is allowed to vary while the height of each bin is constrained so that the area under the PMF approximation is equal to one. The main advantage of EBH over the traditional equidistant histogram (EDH) is that it provides improved resolution in regions where there is a large number of samples. Further, the number of bins b for each histogram considered in this study is set, as suggested in [44], to

$$b = \sqrt{\frac{n}{5}}, \tag{8}$$

where n is the total length of the 1-D vector.

C. TESTING FOR STATISTICAL SIGNIFICANCE IN THE LINEAR/NONLINEAR MEASURES

Testing for the statistical significance is of paramount importance in two scenarios pertaining to this study. Firstly, this test is required to examine the validity of the surrogates for nonlinearity testing (i.e., conformity of the surrogates with $\mathcal{H}_0$). This is achieved through examining the statistical significance of the linearity in the surrogates. If the surrogates are confirmed linear, they are deemed suitable for nonlinearity analysis. Secondly, the statistical significance of the nonlinearity in the original SAR data (i.e., deviation of the original SAR data from $\mathcal{H}_0$) must be tested.

The procedure for testing the significance of the statistic $\mathbb{Q}_S$ is formed by values of $\mathbb{Q}_S$ computed on an ensemble of N surrogates $\{\mathbb{Q}_1, \mathbb{Q}_2, \ldots, \mathbb{Q}_N\}$. Then, if the statistic computed on the original signal, denoted $\mathbb{Q}_0$, is found to be in the tails of the empirical null distribution, $\mathcal{H}_0$ is rejected. This test may be implemented using parametric and nonparametric methods. Both methods are considered in this study to confirm the significance of the results. The parametric test for linearity/nonlinearity is provided in Sect. III-C1, and the nonparametric test for Gaussianity, required to validate the parametric test, is given in Sect. III-C2. Finally, the nonparametric test for linearity/nonlinearity is described in Sect. III-C3.

1) PARAMETRIC TEST FOR LINEARITY/NONLINEARITY

Let $\mathbb{Q}_0$ denote the test statistic generated from the original signal to be tested, $\mathbb{Q}_i$ denote the test statistic for the ith surrogate under $\mathcal{H}_0$, and μ_S and σ_S denote the sample mean and standard deviation, respectively, of the test statistic pertaining to $\mathbb{Q}_S \sim \{\mathbb{Q}_1, \mathbb{Q}_2, \ldots, \mathbb{Q}_N\}$. The parametric measure of statistical significance is defined as

$$\mathcal{L} = \frac{|\mathbb{Q}_0 - \mu_S|}{\sigma_S}. \tag{9}$$

If the distribution of $\mathcal{L}$ is Gaussian, then the P-Value is given by [49] and [50] as

$$P = 1 - \text{erf}\left(\frac{\mathcal{L}}{\sqrt{2}}\right) = \int_{\frac{\mathcal{L}}{\sqrt{2}}}^{\infty} \exp\left(-u^2\right) du. \tag{10}$$

The P-Value represents the probability of observing a significance $\mathcal{L}$ or larger if $\mathcal{H}_0$ is true. Hence, $\mathcal{H}_0$ is rejected if the P-Value is less than or equal to a significance level α (i.e., the alternative hypothesis $\mathcal{H}_1$ is favored). Typically, α is chosen to be either 0.01 or 0.05 [49], [50].

2) NONPARAMETRIC TEST FOR GAUSSIANITY

In order for the parametric test of Sect. III-C1 to be valid, the measure values from the surrogates are assumed to follow the Gaussian distribution. Thus, the parametric test is rendered invalid (or at least inaccurate) if the measure values from the surrogates deviate from the Gaussian distribution. The nonparametric Kolmogorov-Smirnov (KS) test for Gaussianity is considered in this study to examine the conformity of the surrogate statistic ensemble $\{\mathbb{Q}_1, \mathbb{Q}_2, \ldots, \mathbb{Q}_N\}$

with the Gaussian distribution for a significance level α. The KS test achieves this through quantifying the largest vertical distance between the empirical distribution function (EDF) denoted by $\hat{F}(x)$ of the sample and an estimate of the cumulative distribution function (CDF) of the Gaussian distribution denoted by $G(x)$. The KS statistic is given in [51] and [52] as

$$\mathcal{K} = \sup_x \left| \hat{F}(x) - G(x) \right|, \tag{11}$$

where $\sup_x$ is the supremum of the set of distances. An approximation for the critical value pertaining to this test is given by [39], [53]

$$C_\alpha = \frac{K_\alpha}{\sqrt{N} + 0.12 + \frac{0.11}{\sqrt{N}}}, \tag{12}$$

where $K_\alpha = 1.358$ and $K_\alpha = 1.628$ for a significance level $\alpha = 0.05$ and $\alpha = 0.01$, respectively [39], [53]. For a significance level α, Gaussianity is accepted if $\mathcal{K} < C_\alpha$, and the parametric test in Sect. III-C1 is deemed valid. Otherwise, Gaussianity is rejected and the parametric test in Sect. III-C1 is deemed invalid.

3) NONPARAMETRIC TEST FOR LINEARITY/NONLINEARITY

Being distribution-free, the nonparametric approach offers a more robust way to define the statistical significance for linearity/nonlinearity. In this work, a two-sided test is used where $\mathcal{H}_0$ is rejected if $\mathbb{Q}_0$ is smaller than the $\frac{\alpha}{2}$ quantile or larger than the $1 - \frac{\alpha}{2}$ quantile of the surrogate statistic ensemble $\{\mathbb{Q}_1, \mathbb{Q}_2, \ldots, \mathbb{Q}_N\}$. For example, if $N = 1000$ and $\alpha = 0.05$, $\mathcal{H}_0$ is rejected if $\mathbb{Q}_0$ is in the first or last 25 positions of the rank ordered sequence $\{\mathbb{Q}_1, \mathbb{Q}_2, \ldots, \mathbb{Q}_N\}$.

IV. LINEAR TRANSFORMATION OF SAR CHIPS FROM 2-D TO 1-D SPACE

While the linear and nonlinear measures described in Sect. III may be applied to a particular direction in the SAR chip (e.g., vertical, horizontal, diagonal, etc.), it is desired that such measures be designed to account for the neighborhoods of each pixel. Under this section, we propose a method to transform the 2-D SAR chip into an abstract 1-D vector that accounts for the pixel neighborhoods. The method is inspired by the Radon transform. One main advantage of the Radon transform is that, being a linear transform in the spatial-domain, it preserves the original statistics present in the SAR image without introducing any nonlinear artifacts. A succinct description for the forward Radon transform is given in Sect. IV-A. Then, a novel method for linear transformation of the real-valued 2-D SAR chip into a 1-D vector is presented in Sect. IV-B. This is followed, in Sect. IV-C, by a novel method for linear transformation of the bivariate 2-D SAR chip into a 1-D vector. Finally, Sect. IV-D describes a method for linear transformation of the complex-valued 2-D SAR chip into a 1-D vector.

A. THE FORWARD RADON TRANSFORM

The Radon transform $R_\theta\left(x'\right)$ for a 2-D function $f\left(x, y\right)$ is the line integral of f parallel to the y' axis defined, for example in [24], as

$$R_\theta\left(x'\right) = \int_{-\infty}^{\infty} f\left(x' \cos\theta - y' \sin\theta, x' \sin\theta + y' \cos\theta\right) dy',$$

(13)

where θ is the projection angle, and $\left(x', y'\right)$ are the projection coordinates which are related to the projection angle by

$$\begin{bmatrix} x' \\ y' \end{bmatrix} = \begin{bmatrix} \cos\theta & \sin\theta \\ -\sin\theta & \cos\theta \end{bmatrix} \begin{bmatrix} x \\ y \end{bmatrix}.$$

(14)

The geometry of the Radon transform is illustrated in Fig. 1. Note that the $\left(x', y'\right)$ coordinate is rotated (in the spatial-domain) about the center of the image as shown in Fig. 1. An important property of the Radon transform, which is of interest to the study presented in this paper, is linearity [24]. This implies that the Radon transform is both additive and homogeneous. This guarantees that the Radon-transformed signal retains the statistics of the original 2-D SAR chip and does not include nonlinear artifacts due to the transformation process.
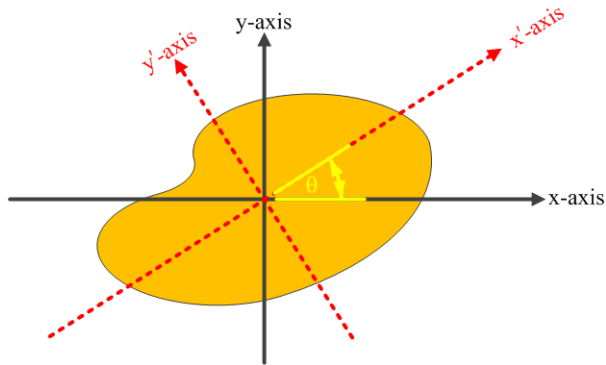

FIGURE 1. Illustration of the Radon transform for a projection angle θ. The random shape provided represents the 2-D function $f\left(x, y\right)$.

B. A METHOD FOR LINEAR TRANSFORMATION OF THE REAL-VALUED 2-D SAR CHIP INTO A 1-D VECTOR

Under this section, a procedure for transforming the real-valued 2-D SAR chip $f\left(x, y\right)$ into a 1-D vector, utilizing the Radon transform, is proposed. The proposed procedure is illustrated in Fig. 2. First, the Radon transform of the
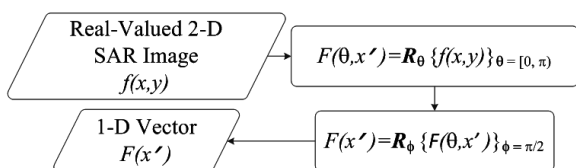

FIGURE 2. Proposed procedure for transforming a real-valued 2-D SAR chip into a 1-D vector.

real-valued input SAR chip is computed for the angles in the interval $[0, \pi)$ as

$$F\left(\theta, x'\right) = R_\theta \left\{f\left(x, y\right)\right\}|_{\theta=[0,\pi)},$$

(15)

a representation known also as a *sinogram*. Note that angles in the range $[\pi, 2\pi]$ are omitted because their corresponding Radon transform provides identical values to the angles in the range $[0, \pi)$, and this redundancy is of no interest to this study. This is followed by integrating out the projection angles $\theta = [0, \pi)$ through applying the Radon transform to the sinogram output at a projection angle $\phi = \frac{\pi}{2}$ to obtain

$$F\left(x'\right) = R_\phi \left\{F\left(\theta, x'\right)\right\}|_{\phi=\frac{\pi}{2}}.$$

(16)

The output given by Eq. 16 is an abstract 1-D vector representative of the input 2-D SAR chip. The procedure shown in Fig. 2 can be applied to any real-valued SAR chip, including the detected SAR chips (i.e., the power and the magnitude-detected chips) as well as the real and the imaginary parts of the complex-valued SAR chip.

C. A METHOD FOR LINEAR TRANSFORMATION OF THE BIVARIATE 2-D SAR CHIP INTO A 1-D VECTOR

Under this section, a procedure for transforming the bivariate SAR chip into a real-valued 1-D vector is proposed. The term bivariate is used here to denote that the real and the imaginary parts of the complex-valued SAR chip are treated as two separate real-valued chips. This is in analogy to the bivariate distribution (e.g., bivariate Gaussian) which is used to model the complex-valued data in such a manner (see [54, p. 20]). The procedure proposed here is meant to account for the bivariate statistics between the real and the imaginary parts of the complex-valued SAR chip. Fig. 3 depicts the proposed procedure.
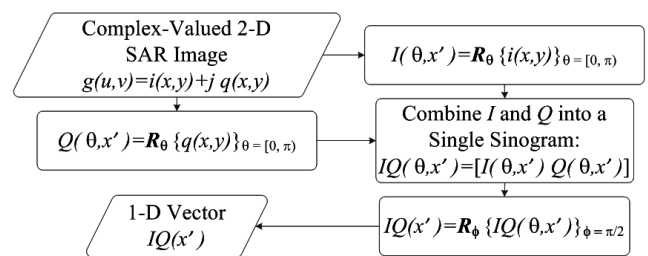
FIGURE 3. Proposed procedure for transforming a bivariate SAR chip into a 1-D vector.

The complex-valued SAR chip is available in the form

$$g\left(u, v\right) = i\left(x, y\right) + j q\left(x, y\right),$$

(17)

where $i\left(x, y\right)$ and $q\left(x, y\right)$ are the real and the imaginary parts, respectively, of the complex-valued SAR chip; and $j = \sqrt{-1}$. Note that (x, y) represent the 2-D Cartesian coordinates of the real-valued plane, while (u, v) represent the 2-D Cartesian coordinates in the complex-valued plane.

The Radon transform is applied separately to the real and the imaginary parts of the complex-valued SAR chip as

$$I\left(\theta, x'\right) = R_\theta \left\{i\left(x, y\right)\right\}\big|_{\theta=[0,\pi)}, \quad (18)$$

$$Q\left(\theta, x'\right) = R_\theta \left\{q\left(x, y\right)\right\}\big|_{\theta=[0,\pi)}. \quad (19)$$

Then, the two sinograms output from Eq. 18 and Eq. 19, respectively, are combined together into a single sinogram as

$$IQ\left(\theta, x'\right) = \left[I\left(\theta, x'\right) \; Q\left(\theta, x'\right)\right]. \quad (20)$$

Note that Matlab notation is used in Eq. 20 to denote that the two sinograms are concatenated horizontally, along the second dimension. Thus, the resultant sinogram has the same number of rows as in the original sinogram (i.e., $I\left(\theta, x'\right)$ and $Q\left(\theta, x'\right)$ have similar size), and the number of columns is doubled. Following this, the projection angles $\theta = [0, \pi)$ are integrated out. This is achieved through applying the Radon transform to the combined sinogram output from Eq. 20 at a projection angle $\phi = \frac{\pi}{2}$ as follows

$$IQ\left(x'\right) = R_\phi \left\{IQ\left(\theta, x'\right)\right\}\big|_{\phi=\frac{\pi}{2}}. \quad (21)$$

The output given by Eq. 21 is an abstract 1-D vector representative of the bivariate statistics in the input 2-D complex-valued SAR chip.

D. A METHOD FOR LINEAR TRANSFORMATION OF THE COMPLEX-VALUED 2-D SAR CHIP INTO A 1-D VECTOR

The procedure described in Sect. IV-C accounts for the bivariate statistics between the real and the imaginary parts of the complex-valued SAR chip. However, the complex-valued statistics [54] are not meant to be accounted for by this procedure. Here, to account for such complex-valued statistics, a simple procedure is proposed. First, the real and the imaginary parts of the complex-valued SAR chip are suitably amalgamated in the spatial-domain according to

$$fu_{iq}\left(x, y\right) = \text{furud}\left(i\left(x, y\right), q\left(x, y\right)\right). \quad (22)$$

This specific form of interleaving is referred to as *furud'ing*, inspired by the spectroscopic binary in the constellation Canis Major known by the traditional name Furud [55], [56]. Fig. 4 illustrates our proposed furud'ing procedure.
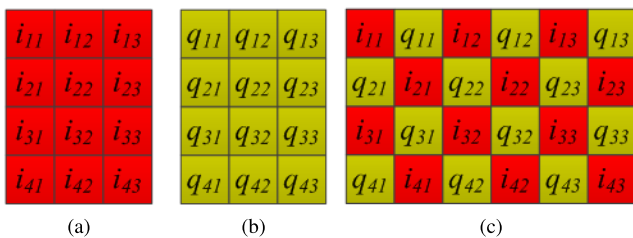

FIGURE 4. Our proposed furud'ing procedure. (a) Real-part of the complex-valued SAR chip, $i\left(x, y\right)$. (b) Imaginary-part of the complex-valued SAR chip, $q\left(x, y\right)$. (c) Furud'ed chip, $fu_{iq}\left(x, y\right)$.

In the next step, the real-valued furud chip is transformed to a 1-D vector through inputting it to the algorithm introduced

in Fig. 2, with the final output being given by

$$Fu_{iq}\left(x'\right) = R_\phi \left\{R_\theta \left\{fu_{iq}\left(x, y\right)\right\}\big|_{\theta=[0,\pi)}\right\}\Big|_{\phi=\frac{\pi}{2}}. \quad (23)$$

V. PROPOSED PROCEDURE FOR NONLINEARITY TESTING IN SAR IMAGERY

Our proposed procedure for nonlinearity testing in SAR imagery is depicted in Fig. 5. Firstly, the 2-D SAR chip is transformed into an abstract 1-D vector, to be used for all subsequent operations, following the procedure described in Sect. IV. Next, an N number of iAAFT surrogates is generated from the abstract 1-D SAR data based on the iAAFT method described in Sect. III-A. Then, the surrogates are tested for linearity. This step is crucial as it guarantees the validity of the iAAFT surrogates for nonlinearity testing in the subsequent stage. The test for linearity commences with computing the PPMC coefficients, at a particular lag τ, for both the input 1-D SAR data as well as for each surrogate, as described by Eq. 6.
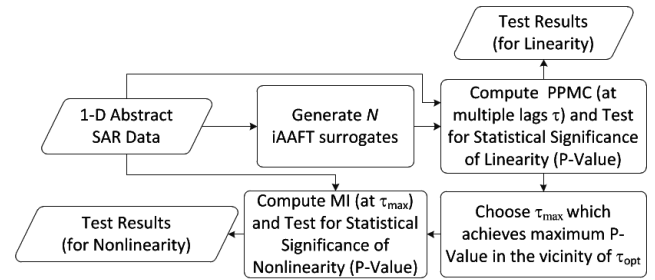
FIGURE 5. Hypothesis test procedure for nonlinearity/linearity proposed in this paper.

Following this, to determine the statistical significance of linearity in the resampled surrogates, the parametric and the nonparametric tests are conducted following the methods described in Sect. III-C1 and Sect. III-C3. Furthermore, in order to validate the parametric test for linearity, the PPMC measure values for the surrogates are also tested for Gaussianity following the KS test described in Sect. III-C2. If the measure values for the surrogates are found to be not strictly Gaussian, the parametric test for linearity is deemed invalid and only the nonparametric test is considered in this case. Otherwise, the P-Values for both the parametric and the nonparametric tests are considered. This procedure is repeated for different lags τ. It is reported in the literature that an approximate optimal value, τ_{opt}, for τ can be chosen such that it corresponds to the first local minimum of the mutual information given by Eq. 7 [43]. However, it should be noted that this value of τ_{opt} is not guaranteed to maximize the linearity in the surrogates. Thus, we choose a value of τ, in the vicinity of τ_{opt}, such that the P-Value for the linearity measures of the N surrogates is maximized and refer to this lag as τ_{max}. This validates the significance for the statistical conformity of the surrogates with $\mathcal{H}_0$. The chosen lag τ_{max} is used in the next stage for testing the nonlinearity.

Finally, to test for the nonlinearity, the MI coefficients, described in Eq. 7, are computed both for the input abstract 1-D SAR data and for the N iAAFT surrogates at lag τ_{max}. Further, both the parametric and the nonparametric tests are conducted to characterize the statistical significance of nonlinearity/linearity (i.e., whichever the test finds to be applicable) in the input abstract 1-D SAR data. The statistical significance for all the results is presented in terms of P-Values. The KS test is applied to the MI coefficients to validate the parametric test as described above.

VI. REAL-WORLD SAR CHIPS

A. SAR CHIPS FROM RADARSAT-2 DATASETS

RS-2 is a spaceborne C-band radar. Two single-channel (HH) single-look complex-valued (SLC) datasets from RS-2 are considered in this study. SLC is the lowest-level product commercially available from MDA Corporation. In the first dataset, the imaging mode is Spotlight. In this mode, RS-2 allows for improved spatial resolution in the azimuth direction in which it delivers the highest nominal spatial resolution of 1.6×0.8 m in range and azimuth, respectively [58]. The targets of interest considered in this dataset are six construction vehicles (shown in red circles in Fig. 6a, and counted from left to right) and one corner reflector (trihedral, shown in red square in Fig. 6a) imaged in a site located in the former Naval Station Argentia in Newfoundland, Canada [57]. The phase image for this scene is provided in Fig. 6b. Ground-truthing is conducted by C-CORE (see Fig. 6c). Note that the size of these targets is comparable to the nominal spatial resolution of the RS-2 sensor (i.e., these targets can be considered as point targets).

In the second dataset, two single-channel SLC SAR chips were extracted from a public-domain RS-2 scene, i.e., Vancouver dataset in [59]. The imaging mode is 'Polarimetric Fine'. Only the HH channel is utilized. The nominal spatial resolution for this imaging mode is 5.2×7.7 m in range and azimuth, respectively [58]. In the first chip, the target is a ship occupies a rectangular area of size 72×34 m in range and azimuth, respectively. Note that this is an extended target. The magnitude-detected chip and the phase chip for this target are provided in Fig. 7. The second chip is pertinent to a target-free sea clutter. The magnitude-detected chip and the phase chip are shown in Fig. 8.

B. SAR CHIPS FROM THE MSTAR DATASET

MSTAR is a public-domain single-channel (HH) and ground-truthed dataset acquired by an airborne SAR sensor. MSTAR offers X-band SLC Spotlight chips for multiple types of military targets (mostly vehicles) imaged under various amounts of articulation, obscuration and camouflage. The MSTAR dataset provides a nominal spatial resolution of 0.3047×0.3047 m in range and azimuth [60]. A set of MSTAR chips pertaining to extended target D7 (bulldozer) is arbitrarily chosen for this study. The chosen set
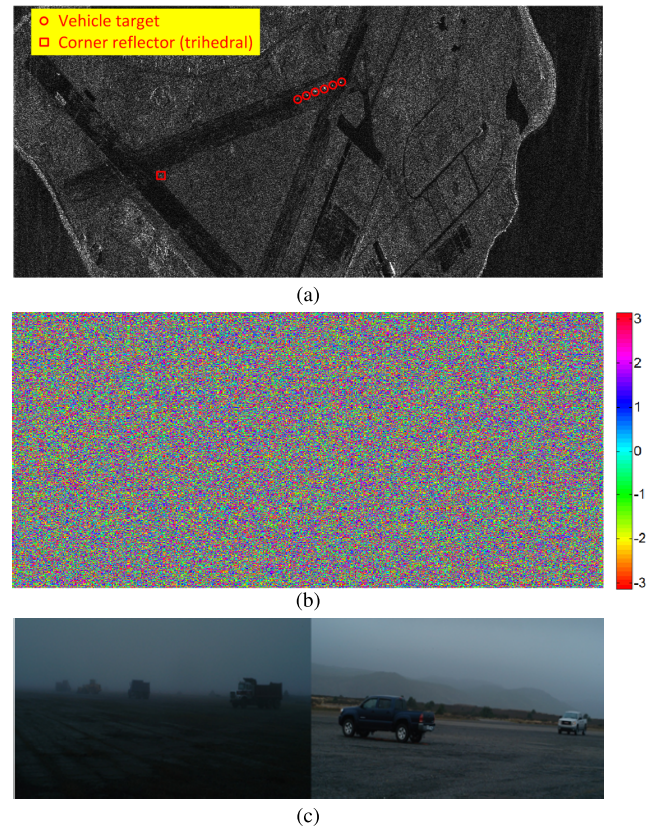
FIGURE 6. Spotlight RS-2 SLC image for a site in the former Naval Station Argentia [57] in Newfoundland, Canada. Ground-truth image is provided by C-CORE. RADARSAT-2 Data and Products©MacDonald, Dettwiler and Associates Ltd. (2011). (a) Contrast-enhanced and magnitude-detected RS-2 image. Vehicle targets are numbered 1 to 6, respectively, from left to right. The corner reflector is referred to as CR. (b) Phase image. (c) Ground-truth image (left to right: 1 dump truck, 1 loader, 2 dump trucks, 2 pickup trucks).
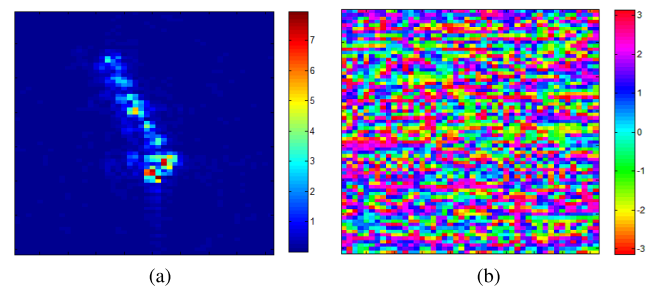
FIGURE 7. RS-2 chip for ocean-based extended (ship) target (ET). RADARSAT-2 Data and Products©MacDonald, Dettwiler and Associates Ltd. (2008). (a) Magnitude-detected chip. (b) Phase chip.

is representative of different azimuth angles for this target. Table 1 provides a list of the chosen MSTAR chip IDs along with relevant azimuth angles. A ground-truth image for the target is shown in Fig. 9. The magnitude-detected images for all the MSTAR chips of target D7 considered in this paper, are provided in Fig. 10. The corresponding

(a)   (b)
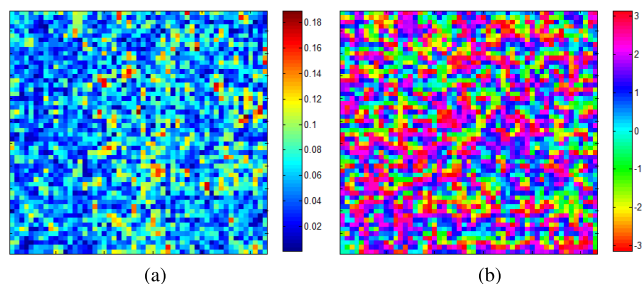
FIGURE 8. RS-2 chip for ocean clutter (i.e., target-free (TF) chip). RADARSAT-2 Data and Products©MacDonald, Dettwiler and Associates Ltd. (2008). (a) Magnitude-detected chip. (b) Phase chip.

TABLE 1. List of the MSTAR chips of target D7 used in this paper.

No.	MSTAR ID	Azimuth Angle
1	HB15056.005	13.307442°
2	HB15256.005	36.307442°
3	HB15132.005	94.307442°
4	HB14931.005	97.307442°
5	HB15006.005	113.307442°
6	HB15206.005	121.307442°
7	HB15082.005	144.307434°
8	HB15148.005	180.307434°
9	HB15156.005	220.307434°
10	HB14956.005	222.307434°
11	HB15031.005	243.307434°
12	HB15231.005	261.307434°
13	HB15106.005	274.307434°
14	HB14981.005	347.307434°
15	HB15181.005	350.307434°

FIGURE 9. Ground-truth image for target D7.

phase chips are depicted in Fig. 11. The numbers shown on the chips represent the chip number provided in Table 1.

C. SAR CHIPS FROM A VERY HIGH-RESOLUTION SENSOR

The final two SAR chips considered in this study are from a very high-resolution single-channel X-band SAR system, obtained from [61] and [62]. The imaging mode is 'Stripmap'. The nominal spatial resolution of the SAR sensor is 0.03 × 0.012 m in range and azimuth, respectively. The first target is a bike. The magnitude-detected and phase chips for this target are shown in Fig. 12. The second target is the phrase GO STATE which is formed through using a group of tiny pushpins. The magnitude-detected and phase chips for this target are depicted in Fig. 13.
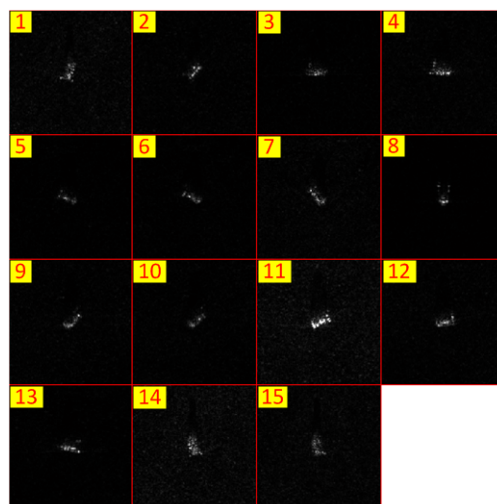
FIGURE 10. Magnitude-detected chips for a selected set from MSTAR target D7.
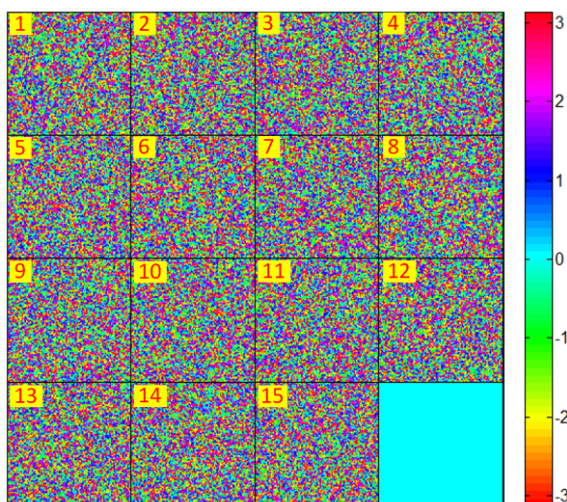
FIGURE 11. Phase chips for a selected set from MSTAR target D7.

(a)   (b)
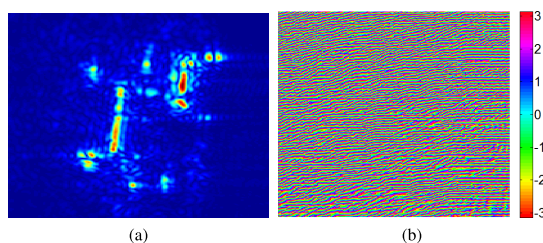
FIGURE 12. SAR chip for a bike from a very high-resolution X-band radar. (a) Magnitude-detected chip for a bike. (b) Phase chip for a bike.

VII. RESULTS AND COMMENTS

A. APPLICABILITY OF THE GCLT THEOREM TO SAR IMAGERY, AND THE INTERRELATIONSHIP WITH THE SPATIAL RESOLUTION

This section aims at empirically demonstrating the inapplicability of the CLT theorem to the extended targets in SAR imagery. Further, the effect of the spatial resolution for the SAR sensor is also examined. Five complex-valued SAR
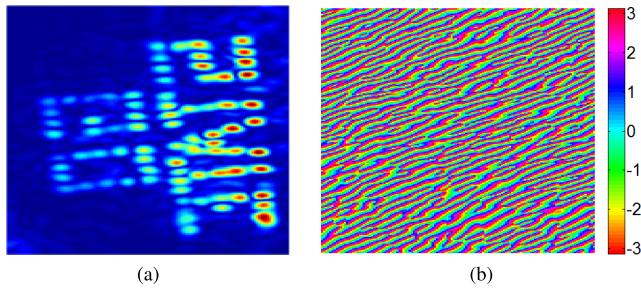
FIGURE 13. SAR chip for GO STATE in pushpins from a very high-resolution X-band radar. (a) Magnitude-detected chip for GO STATE in pushpins. (b) Phase chip for GO STATE in pushpins.

FIGURE 14. Histogram and fitting with Gaussian and GGD distributions for ocean clutter (i.e., target-free (TF) chip). (a) Histogram for real-part. (b) GGD PDF and Gaussian PDF superimposed on histogram of real-part in Fig. 14a. (c) Histogram for imaginary-part. (d) GGD PDF and Gaussian PDF superimposed on histogram of imaginary-part in Fig. 14c.

chips containing a variety of target types and having differing spatial resolutions are chosen. The first chip is for target-free (i.e., TF) ocean clutter taken from the RS-2 dataset introduced in Sect. VI-A. The second chip containing target #1 and representing the case of a point target, is taken from the RS-2 dataset introduced in Sect. VI-A. The third chip is for target ET taken from the RS-2 dataset introduced in Sect. VI-A. This chip represents the case of an extended target. The fourth chip is for target #11 taken from the MSTAR dataset presented under Sect. VI-B. This chip also represents an extended target. Finally, the fifth chip is for the phrase GO STATE in pushpins given under Sect. VI-C. This case too represents an extended target. For each of these chips, the following procedure is applied. First, a normalized EDH histogram is computed for both the real-part and the imaginary-part, respectively. Then, the envelope of the resultant histogram is fitted to the Gaussian distribution and the GGD distribution, respectively. The Gaussian distribution serves to demonstrate the applicability/inapplicability of the CLT theorem. The GGD distribution is a non-Gaussian statistical model motivated by the GCLT theorem. GGD allows the rate of tail decay to be varied and it is known to offer a good model for some impulsive phenomena. The GGD family is general in that it encompasses a wide array of distributions with different tail characteristics from super-Gaussian to sub-Gaussian with specific densities such as Laplacian and Gaussian distributions [17], [63]. The GGD distribution is chosen in this study because it is found to closely fit our SAR data.

Fitting with the Gaussian distribution is performed using the minimum variance unbiased estimator (MVUE) [64]. Fitting with the GGD distribution is done through minimizing the symmetrized relative entropy, known as the Jensen–Shannon (JS) divergence, between the envelope of the histogram and the GGD's PDF (see [4] and Eq. 30 in Appendix for details). Goodness-of-fit measures between the normalized histograms and both the Gaussian and the GGD PDFs are presented in terms of the JS divergence (see Eq. 30 in Appendix for details). Our results are presented in Fig. 14-Fig. 18, respectively. Goodness-of-fit measures are given in Table 2.

The following conclusions are drawn based on the results obtained. First, for the target-free RS-2 chip considered, it is
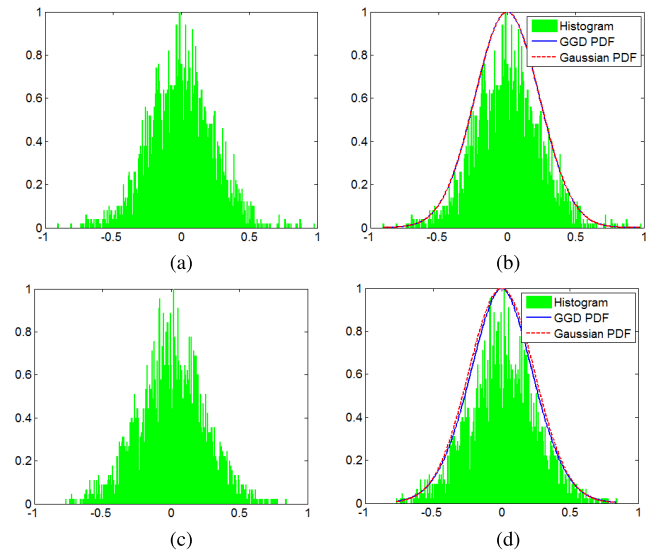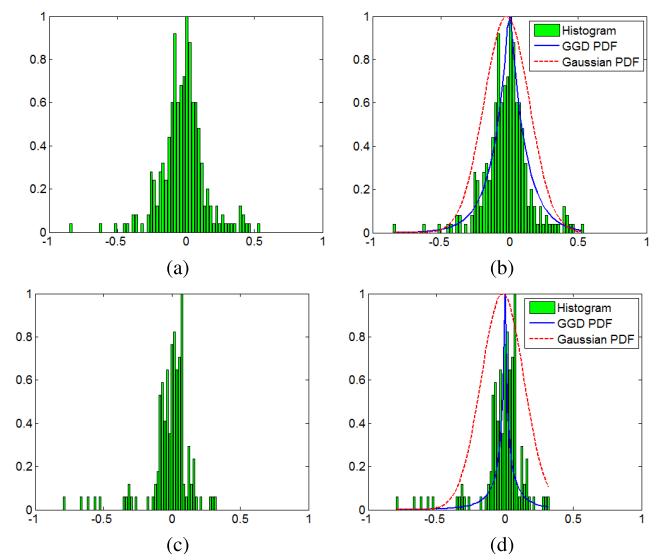
FIGURE 15. Histogram and fitting with Gaussian and GGD distributions for RS-2 target #1. (a) Histogram for real-part. (b) GGD PDF and Gaussian PDF superimposed on histogram of real-part in Fig. 15a. (c) Histogram for imaginary-part. (d) GGD PDF and Gaussian PDF superimposed on histogram of imaginary-part in Fig. 15c.

evident that the goodness-of-fit for both the Gaussian and the GGD PDFs are almost identical (see Fig. 14 and Table 2). It is thus concluded that nonlinearity is negligible in the absence of targets. Second, based on the fitting results for the case of point target considered (see Fig. 15 and Table 2), the Gaussian PDF and the GGD PDF are close to each other (i.e., in terms of the JS divergence), despite the relatively better fit achieved by the GGD PDF. It is observed that the GGD
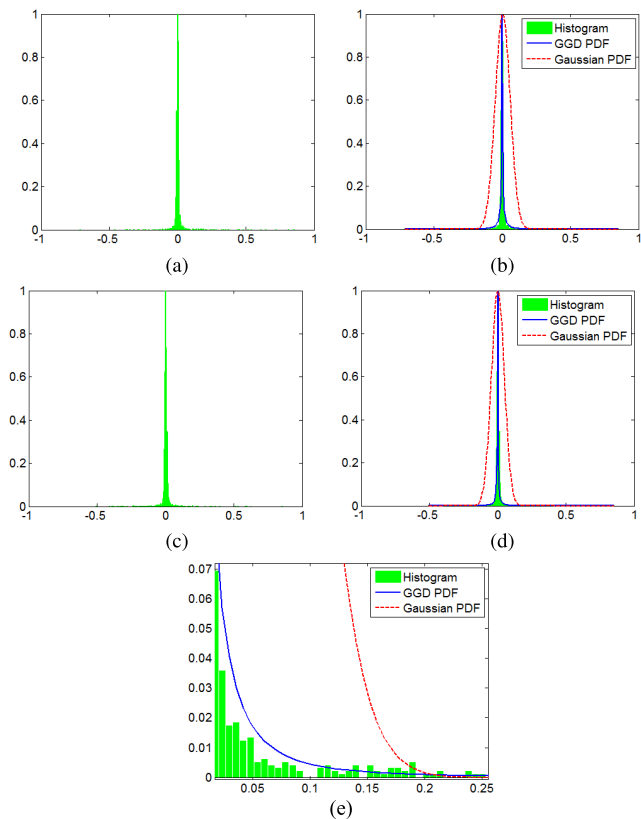
FIGURE 16. Histogram and fitting with Gaussian and GGD distributions for RS2 extended (ship) target (ET). (a) Histogram for real-part. (b) GGD PDF and Gaussian PDF superimposed on histogram of real-part in Fig. 16a. (c) Histogram for imaginary-part. (d) GGD PDF and Gaussian PDF superimposed on histogram of imaginary-part in Fig. 16c. (e) Zoom-in into the right tail of Fig. 16b.

FIGURE 17. Histogram and fitting with Gaussian and GGD distributions for MSTAR target #11. (a) Histogram for real-part. (b) GGD PDF and Gaussian PDF superimposed on histogram of real-part in Fig. 17a. (c) Histogram for imaginary-part. (d) GGD PDF and Gaussian PDF superimposed on histogram of imaginary-part in Fig. 17c. (e) Zoom-in into the right tail of Fig. 17b.

PDF gives more weight to the heavy tails and peakedness of the histogram while the Gaussian PDF is restricted by the sample variance. Note that the smaller the JS divergence measure is, the better the fit. Thus, it is evident that the point target considered also possesses minimum nonlinearity. Third, for all the other chips considered, the GGD distribution offers a much better fit than the Gaussian distribution. This is evident through visually inspecting the fitting results depicted in Fig. 16-Fig. 18, respectively. This is also confirmed from Table 2 for the JS divergence measures. It is clear that the Gaussian distribution cannot model pulsed phenomenon with heavy tails (i.e., super-Gaussian) similar to those obtained in the figures pertinent to the case of extended targets. However, the GGD distribution accounts for this behavior. Further, it is noted that the peakedness and the heavy tails get even more pronounced with the increase in the spatial resolution of the SAR sensor relative to the size of the imaged target. This is clearly observed through comparing the histograms in Fig. 18 with Fig. 16 and Fig. 17, respectively. This behavior increases the goodness-of-fit between the histogram and the GGD PDF, in contrast to the Gaussian PDF. This is confirmed by examining the JS divergence measures provided in Table 2.

Since the Gaussian distribution motivates the CLT theorem, this demonstrates the inapplicability of the CLT theorem to the real-part and the imaginary-part of the SAR chips containing the extended targets. Similarly, since the GGD distribution is motivated by the GCLT theorem, it can be said that in the presence of extended targets, the SAR chips considered demonstrate some nonlinear behavior. This nonlinear behavior becomes even more pronounced with the increase in the spatial resolution of the SAR sensor, relative to the size of the imaged target. The statistical significance of the nonlinearity is investigated in the next section.

B. STATISTICAL ANALYSIS FOR NONLINEARITY
This section presents the statistical analysis results for the nonlinear dynamics in the SAR datasets introduced under Sect. VI. This analysis follows the procedure described under Sect. V. The analysis utilizes a number of 1024 iAAFT surrogates (i.e., $N = 1024$) for each 1-D vector representation. The number 1024 is chosen as a tradeoff between computational complexity and statistical significance. Once the iAAFT surrogates are calculated, the spatial lag τ_{max} is found for each 1-D vector representation. Then, the nonlinear measures in terms of MI, are calculated
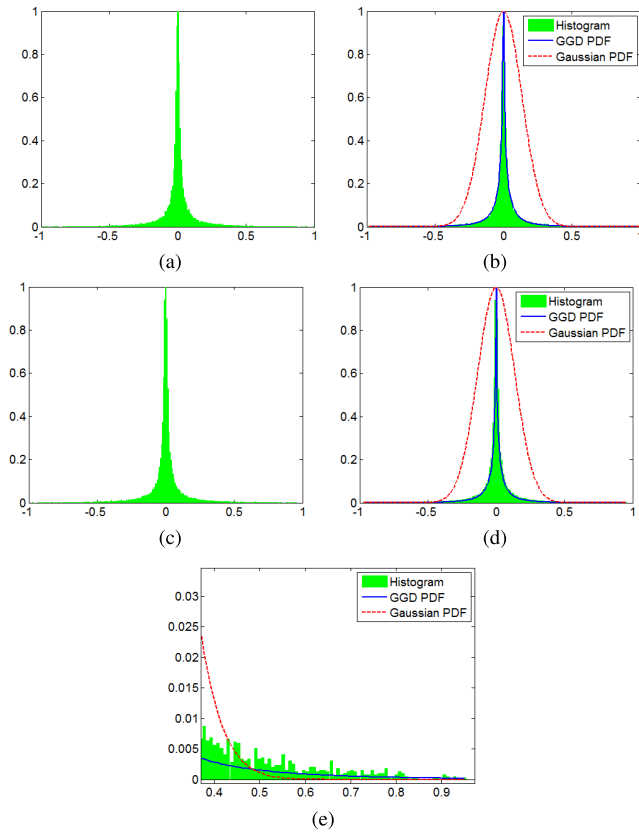
FIGURE 18. Histogram and fitting with Gaussian and GGD distributions for the SAR chip of GO STATE in pushpins. (a) Histogram for real-part. (b) GGD PDF and Gaussian PDF superimposed on histogram of real-part in Fig. 18a. (c) Histogram for imaginary-part. (d) GGD PDF and Gaussian PDF superimposed on histogram of imaginary-part in Fig. 18c. (e) Zoom-in into the right tail of Fig. 18b.

TABLE 2. Goodness-of-fit measures for Fig. 14-Fig. 18, respectively.

Chip	Spatial Resolution [Range × Azimuth]	Target Type	Channel	JS Divergence Gaussian PDF	JS Divergence GGD PDF
RS2 TF	[0.3047 × 0.3047] m	Ocean Clutter	I	0.0592	0.0590
			Q	0.0625	0.0605
RS2 #1	[1.6 × 0.8] m	Point Target	I	0.2204	0.1218
			Q	0.4678	0.3944
RS2 ET	[5.2 × 7.7] m	Extended Target	I	2.0096	0.2277
			Q	1.8840	0.2839
MSTAR #11	[0.3047 × 0.3047] m	Extended Target	I	0.8886	0.2495
			Q	0.7589	0.1624
GO STATE	[0.03 × 0.012] m	Extended Target	I	0.7667	0.0353
			Q	0.7671	0.0384

at τ_{max} for each 1-D representation and its corresponding 1024 iAAFT surrogates. Parametric and nonparametric tests for the statistical significance pertinent to both the linearity of the surrogates (i.e., in terms of PPMC) and the non-linearity of the 1-D representations (i.e., in terms of MI) are presented in terms of P-Values following the procedure outlined in Sect. III-C1 and Sect. III-C3, respectively. The applicability of the parametric test is validated following the procedure presented in Sect. III-C2.

The statistical analysis results for the SAR chips from the RS-2 dataset are presented in Table 3. The results pertaining to the SAR chips from the MSTAR dataset are provided in Table 4. Finally, Table 5 and Table 6 respectively present the statistical analysis results for the two chips from the very high-resolution SAR dataset.

TABLE 3. Nonlinearity analysis of the RS-2 chips. GR means Gaussianity Rejected.

No.	Type	τ	PPMC (P-Value) Parametric	PPMC (P-Value) Nonparametric	MI (P-Value) Parametric	MI (P-Value) Nonparametric
CR	P	4	GR	0.9317	GR	0.3015
	M	12	GR	0.9902	GR	0.9278
	I	6	GR	0.9376	GR	0.7073
	Q	11	GR	0.7932	GR	0.1063
	IQ	19	GR	0.8595	GR	0.2234
	Fu$_{iq}$	15	GR	0.9473	GR	0.0634
1	P	8	GR	0.9668	GR	0.6527
	M	13	GR	0.8966	GR	0.9376
	I	6	GR	0.2605	GR	0.9005
	Q	3	GR	0.6859	GR	0.3405
	IQ	20	GR	0.9220	GR	0.3990
	Fu$_{iq}$	7	GR	0.3600	GR	0.5141
2	P	7	GR	0.9863	GR	0.6273
	M	8	GR	0.9766	GR	0.9356
	I	3	GR	0.9590	GR	0.6898
	Q	2	GR	0.8263	GR	0.4693
	IQ	1	GR	0.9220	GR	0.2839
	Fu$_{iq}$	10	GR	0.6293	GR	0.6956
3	P	6	GR	0.9454	GR	0.5434
	M	9	GR	0.9356	GR	0.9434
	I	9	GR	0.8751	GR	0.9571
	Q	12	GR	0.7854	GR	0.3015
	IQ	6	GR	0.9649	GR	0.7873
	Fu$_{iq}$	20	GR	0.9629	GR	0.7229
4	P	6	GR	0.9688	GR	0.7483
	M	9	GR	0.8771	GR	0.8810
	I	9	GR	0.8927	GR	0.2078
	Q	6	GR	0.9863	GR	0.2878
	IQ	5	GR	0.9805	GR	0.3288
	Fu$_{iq}$	12	GR	0.8107	GR	0.4498
5	P	13	GR	0.8888	GR	0.8556
	M	13	GR	0.9649	GR	0.9902
	I	8	GR	0.9278	GR	0.7795
	Q	6	0.8029	0.8459	GR	0.0654
	IQ	10	GR	0.8595	GR	0.2898
	Fu$_{iq}$	2	GR	0.9317	GR	0.0927
6	P	12	GR	0.9395	GR	0.7854
	M	14	GR	0.9707	GR	0.9317
	I	18	GR	0.9766	GR	0.5805
	Q	6	GR	0.4400	GR	0.4985
	IQ	20	GR	0.9220	GR	0.5298
	Fu$_{iq}$	2	GR	0.7346	GR	0.9571
ET	P	4	GR	0.9707	0.0000	0.0010
	M	5	GR	0.7854	0.0216	0.0244
	I	5	GR	0.9044	0.0033	0.0049
	Q	9	GR	0.8576	GR	0.0556
	IQ	4	GR	0.7034	0.0014	0.0010
	Fu$_{iq}$	4	GR	0.4966	0.0000	0.0010
TF	P	6	GR	0.6468	GR	0.4322
	M	7	GR	0.5317	GR	0.2546
	I	5	GR	0.8439	GR	0.0088
	Q	5	GR	0.8673	0.1921	0.2098
	IQ	11	GR	0.7073	GR	0.8790
	Fu$_{iq}$	12	GR	0.7054	0.6191	0.6585

C. COMMENTS

Firstly, through inspecting the results for the RS-2 dataset presented in Table 3, it is clear that the statistical significance for the nonlinearity is dependent on the target size relative to the spatial resolution of the SAR sensor. It is observed that the nonlinearity is negligible for all the point targets considered (i.e., construction vehicles and CR) as well as for the target-free ocean clutter chip. This can be inferred through examining the P-Values under the MI measures. To reiterate,

$$\text{Linearity: } \mathcal{H}_0 \in \text{P-Value} > 0.01, \quad (24)$$

$$\text{Nonlinearity: } \mathcal{H}_1 \in \text{P-Value} \leq 0.01. \quad (25)$$

TABLE 4. Nonlinearity analysis of the MSTAR chips.

No.	Type	τ	PPMC (P-Value) Parametric	Nonparametric	MI (P-Value) Parametric	Nonparametric
1	P	5	GR	0.7268	GR	0.0010
	M	6	GR	0.7268	0.1406	0.1239
	I	8	GR	0.9239	GR	0.0127
	Q	9	GR	0.7678	GR	0.0283
	IQ	6	GR	0.6644	GR	0.0010
	Fu_{iq}	9	GR	0.9278	GR	0.0907
2	P	3	GR	0.8829	GR	0.0010
	M	12	GR	0.8498	0.1290	0.1063
	I	3	GR	0.9532	GR	0.0010
	Q	12	GR	0.5083	GR	0.0576
	IQ	4	GR	0.3015	GR	0.0302
	Fu_{iq}	10	GR	0.4810	GR	0.0088
3	P	1	GR	0.8732	GR	0.0010
	M	10	GR	0.8888	0.0581	0.0576
	I	3	GR	0.9707	GR	0.0029
	Q	7	GR	0.9941	0.0000	0.0010
	IQ	3	GR	0.9063	GR	0.0010
	Fu_{iq}	10	GR	0.7580	GR	0.0010
4	P	6	GR	0.9434	GR	0.0010
	M	12	GR	0.8498	0.0273	0.0302
	I	12	GR	0.8439	GR	0.1961
	Q	8	GR	0.6644	GR	0.0010
	IQ	14	GR	0.9063	GR	0.0068
	Fu_{iq}	12	GR	0.1220	GR	0.0029
5	P	5	GR	0.9766	GR	0.0010
	M	14	GR	0.9298	0.0148	0.0146
	I	17	GR	0.9337	0.1680	0.1571
	Q	7	GR	0.8166	GR	0.0010
	IQ	13	GR	0.7151	GR	0.0888
	Fu_{iq}	6	GR	0.7502	GR	0.0615
6	P	4	GR	0.9473	GR	0.0010
	M	9	GR	0.9844	0.0541	0.0380
	I	4	GR	0.4849	GR	0.0068
	Q	4	GR	0.4010	GR	0.0088
	IQ	4	GR	0.2117	GR	0.0010
	Fu_{iq}	3	GR	0.1298	GR	0.0010
7	P	6	GR	0.5063	0.0000	0.0010
	M	5	GR	0.7307	0.0413	0.0380
	I	4	GR	0.3307	GR	0.0537
	Q	7	GR	0.2702	GR	0.0029
	IQ	4	GR	0.6605	GR	0.0146
	Fu_{iq}	5	GR	0.3210	GR	0.0010
8	P	13	GR	0.8732	GR	0.0010
	M	3	GR	0.5044	GR	0.0010
	I	3	GR	0.9395	GR	0.0185
	Q	1	GR	0.8810	GR	0.0010
	IQ	2	GR	0.3249	GR	0.0029
	Fu_{iq}	4	GR	0.9024	GR	0.0010
9	P	6	GR	0.5161	GR	0.0010
	M	12	GR	0.9063	0.1155	0.0888
	I	7	GR	0.7463	GR	0.0010
	Q	10	GR	0.5922	GR	0.0049
	IQ	10	GR	0.8771	GR	0.0049
	Fu_{iq}	17	GR	0.8537	GR	0.0166
10	P	3	GR	0.9200	GR	0.0010
	M	12	GR	0.8341	0.0572	0.0634
	I	5	GR	0.3034	GR	0.0010
	Q	3	GR	0.8341	GR	0.0166
	IQ	4	GR	0.1688	GR	0.0166
	Fu_{iq}	6	GR	0.5688	GR	0.0010
11	P	2	GR	0.9727	GR	0.0010
	M	11	GR	0.8732	0.0437	0.0556
	I	4	GR	0.5922	GR	0.0068
	Q	4	GR	0.8400	GR	0.0010
	IQ	6	GR	0.3951	GR	0.0010
	Fu_{iq}	8	GR	0.3268	GR	0.0029
12	P	7	GR	0.9278	0.0000	0.0010
	M	10	GR	0.8615	0.1059	0.1024
	I	10	GR	0.8478	GR	0.0810
	Q	8	GR	0.7951	GR	0.0010
	IQ	8	GR	0.6078	0.0000	0.0010
	Fu_{iq}	14	GR	0.5337	0.0000	0.0029
13	P	2	GR	0.9590	GR	0.0010
	M	9	GR	0.9180	0.0408	0.0459
	I	2	GR	0.9941	GR	0.0029
	Q	4	GR	0.7620	GR	0.0068
	IQ	2	GR	0.8556	GR	0.0010
	Fu_{iq}	5	GR	0.9434	GR	0.0127
14	P	4	GR	0.5220	GR	0.0010
	M	12	GR	0.7015	0.5185	0.5317
	I	8	GR	0.8556	GR	0.0010
	Q	17	GR	0.8537	GR	0.0068
	IQ	11	GR	0.8946	GR	0.0537
	Fu_{iq}	16	GR	0.9434	GR	0.0107
15	P	4	GR	0.9668	GR	0.0010
	M	5	GR	0.6351	0.0815	0.0654
	I	9	GR	0.9688	GR	0.0010
	Q	17	GR	0.9941	GR	0.5532
	IQ	13	GR	0.9844	GR	0.0634
	Fu_{iq}	12	GR	0.5668	GR	0.0049

TABLE 5. Nonlinearity analysis of the SAR chip for a bike.

Type	τ_{max}	PPMC (P-Value) Parametric	Non-Parametric	MI (P-Value) Parametric	Non-Parametric
P	19	GR	0.9532	0.0000	0.0010
M	20	GR	0.4498	0.2070	0.2351
I	2	GR	0.7659	0.0000	0.0010
Q	2	GR	0.7971	0.0052	0.0068
IQ	2	GR	0.8185	0.0000	0.0010
Fu_{iq}	9	GR	0.9551	0.000	0.0010

TABLE 6. Nonlinearity analysis of the SAR chip for GO STATE in pushpins.

Type	τ_{max}	PPMC (P-Value) Parametric	Non-Parametric	MI (P-Value) Parametric	Non-Parametric
P	16	GR	0.9317	0.0795	0.0888
M	14	GR	0.6332	0.1156	0.1337
I	2	GR	0.5883	GR	0.0010
Q	2	GR	0.7307	GR	0.0010
IQ	2	GR	0.6351	GR	0.0010
Fu_{iq}	8	GR	0.8751	GR	0.0010

is orders of magnitude greater than the spatial resolution of the RS-2 sensor. For all the RS-2 target chips analyzed it is noted that the MI's P-Value pertaining to the power-detection is less than that of the magnitude-detection, and different from that of the real and the imaginary parts. This indicates that both the power and the magnitude detections alter the statistics in the original SAR image with a more pronounced effect observed for the magnitude detection. This is in agreement with previous investigations into the effect of power and magnitude detections on complex-valued SAR imagery (see [5], [8], [9], [65] and [5, Sec. 2.8²]).

Next, from Table 4 it is evident that the nonlinearity behavior in the complex-valued MSTAR dataset is statistically significant. This is to be expected since the imaged objects are all extended targets. It can be seen that the smallest MI's P-Value alternates between the real and the imaginary parts which indicates that the nonlinearity effect originates from both of these parts. A close look at the effect of detection in terms of P-Values reveals that magnitude-detection is worst when it comes to either greatly diminishing or obliterating the nonlinear dynamics originally present in the complex-valued SAR chip. This is in agreement with the results for the RS-2 dataset. The power-detected SAR chip retains some of the nonlinear characteristics present in the real and the imaginary parts. However, through visually comparing the 1-D representations for the undetected and the power-detected SAR chips, it is postulated that the nonlinear dynamics have been altered from their original form. Furthermore, it is also suggested that although the 1-D representation for the real-part, imaginary-part, bivariate and furud'ed representations, respectively, do possess some nonlinear behavior, the

Moreover, when an extended target for a ship of size of 72×34 m is considered, the nonlinear dynamics are found to become pronounced. This is expected since the ship size

---

²"*Power detection* widens the signal bandwidth by a factor of two. *Magnitude detection* involves a further square root operation. The magnitude detection creates spectral components with a bandwidth wider than twice the bandwidth of the original complex signal [5]."

nonlinear dynamics in these different representations are not identical.

In addition to the foregoing observations, the results obtained from the very high-resolution SAR dataset given in Table 5 and Table 6, respectively, evidently reveal a significant nonlinear trend. This can be attributed to the fact that the imaged objects are extended targets. The nonlinear effect is clearly manifested through noting that all the MI's P-Values for the real-part, imaginary-part, bivariate and furud'ed representations, respectively, strongly favor $\mathcal{H}_1$ for the nonlinearity. Similarly, it is observed that the magnitude-detection greatly diminishes the nonlinear effects originally present in the complex-valued SAR chip. While the power-detection often retains some of the nonlinear characteristics in an altered form, it is noted that this may not be the case at very high-resolution and for the relatively small targets such as that of GO STATE in pushpins (see Table 6).

Finally, several overall observations may be summarized. The nonlinear effects in complex-valued SAR chips are proportional to the spatial resolution and the size of the imaged target. Magnitude-detection greatly diminishes or obliterates the nonlinear effects. Power-detection either diminishes or alters the nonlinear effects. Further, as reported in [4], for the case of extended targets, the complex-valued SAR chip is inherently noncircular (i.e., the phase is informative). This implies that full information about the nonlinear dynamics is preserved in the complex-valued SAR chip and not in the detected one. It may be noted that target recognition in SAR imagery is an important application of the nonlinear phenomenon. Previous research has empirically observed that 'nonlinear dynamics' are dependent on the target type and the operating conditions at which the target is imaged [4], [7]–[9]. Accordingly, through developing suitable techniques to harness the 'nonlinear dynamics' in complex-valued SAR imagery, relevant target recognition applications are naturally expected to achieve improvement in target discrimination accuracy. Hence, to take full advantage of the nonlinear statistics for the extended targets, it is advised to utilize the complex-valued SAR image rather than the detected one. It may be useful to consider the real-part, imaginary-part, bivariate and furud'ed 1-D representations as complementary to each other. The 1-D representations for the real and the imaginary parts capture the nonlinear dynamics in the 2-D counterparts. The bivariate representation captures the bivariate nonlinear dynamics between the real and the imaginary parts. The furud'ed representation accounts for the nonlinear dynamics both within and between the pixels of the real and the imaginary parts.

VIII. CONCLUSIONS

This paper has introduced a systematic procedure to infer the statistical significance of the nonlinear dynamics in complex-valued SAR imagery. The applicability of the proposed procedure is demonstrated on various real-world target chips from multiple SAR sensors having a variety of spatial resolutions. The analysis confirms the statistical significance

of the nonlinear phenomenon in the complex-valued SAR chip for the case of extended targets. Furthermore, as the complex-valued SAR chip is magnitude-detected, the nonlinear effect is either obliterated or greatly diminished. The power-detected chip is found to retain some nonlinear statistics, though altered from their original form present in the complex-valued chip. Additionally, both power and magnitude detections obliterate the information about noncircularity present only in the complex-valued SAR chip [4]. Hence, for the case of extended targets, to take full advantage of the nonlinear dynamics in applications such as target recognition, it is recommended to utilize the complex-valued SAR image rather than the detected one. This paper has been extended in [66] where a new framework for feature extraction, based on the 1-D representations developed in this work, is presented. This provides for harnessing the nonlinear dynamics embedded in the complex-valued SAR chip. Features utilizing the nonlinear dynamics are compared with baseline features extracted from the power-detected SAR chip. The unique advantage of the nonlinear dynamics for target classification SAR imagery is clearly demonstrated.

APPENDIX

In order to measure the goodness-of-fit between the empirical histogram (i.e., p) and the PDF obtained based on the estimation of parameters (i.e., q), a symmetrized version of Kullback–Leibler (KL) divergence (also known as the relative entropy) is used. The KL divergence is an information-theoretic approach that measures the information lost when $q(x)$ is used to estimate $p(x)$. The KL divergence of $q(x)$ from $p(x)$ is given by [67]

$$KLD\,(p||q) = \sum_{x \in X} p\,(x) \log_2 \left(\frac{p\,(x)}{q\,(x)} \right). \qquad (26)$$

The KL divergence provides a means for comparing the entropy of the two distributions over the same random variable X. Intuitively, this allows for estimating the number of additional bits required when encoding a random variable X with a distribution $p(x)$ using the alternative distribution $q(x)$. The properties of interest pertaining to the KL divergence are

$$KLD\,(p||q) \geq 0, \qquad (27)$$
$$KLD\,(p||q) = 0 \quad \text{iff } p\,(x) = q\,(x) \text{ for all } x \in X, \quad (28)$$
$$KLD\,(p||q) \neq KLD\,(q||p), \qquad (29)$$

Jensen–Shannon (JS) divergence is a symmetrized version of KL divergence. It is calculated as [68], [69]

$$JSD = \frac{KLD\,(p||q) + KLD\,(q||p)}{2}. \qquad (30)$$

ACKNOWLEDGMENTS

REFERENCES

[1] C. P. Silva, "Nonlinear dynamics and chaos: From concept to application," *Crosslink Mag.*, vol. 12, no. 1, pp. 40–51, 2011. [Online]. Available: http://www.aerospace.org/wp-content/uploads/crosslink/V12N1.pdf

[2] (2015). *The Society for Nonlinear Dynamics and Econometrics*. [Online]. Available: http://www.sndeecon.org/home/home.html

[3] S. H. Strogatz, *Nonlinear Dynamics and Chaos: With Applications to Physics, Biology, Chemistry, and Engineering* (Studies in Nonlinearity). Reading, MA, USA: Perseus Books, 1994.

[4] K. El-Darymli, P. McGuire, E. W. Gill, D. Power, and C. Moloney, "Characterization and statistical modeling of phase in single-channel synthetic aperture radar imagery," *IEEE Trans. Aerosp. Electron. Syst.*, to be published.

[5] I. G. Cumming and F. H. Wong, *Digital Signal Processing of Synthetic Aperture Radar Data: Algorithms and Implementation*. Norwood, MA, USA: Artech House, 2004.

[6] C. Oliver and S. Quegan, *Understanding Synthetic Aperture Radar Images*. Raleigh, NC, USA: SciTech Publishing, 2004.

[7] A. Rihaczek and S. J. Hershkowitz, "Man-made target backscattering behavior: Applicability of conventional radar resolution theory," *IEEE Trans. Aerosp. Electron. Syst.*, vol. 32, no. 2, pp. 809–824, Apr. 1996. [Online]. Available: http://dx.doi.org/10.1109/7.489523

[8] A. W. Rihaczek and S. J. Hershkowitz, *Radar Resolution and Complex-Image Analysis*. Norwood, MA, USA: Artech House, 1996.

[9] A. W. Rihaczek and S. J. Hershkowitz, *Theory and Practice of Radar Target Identification*. Boston, MA, USA: Artech House, 2000.

[10] K. El-Darymli, C. Moloney, E. Gill, P. McGuire, and D. Power, "Recognition of nonlinear dispersive scattering in SAR imagery," in *Proc. IEEE IGARSS*, Quebec City, QC, Canada, Jul. 2014, pp. 4722–4725. [Online]. Available: http://dx.doi.org/10.1109/IGARSS.2014.6947548

[11] K. El-Darymli, "Holism for target recognition in synthetic aperture radar imagery," Ph.D. dissertation, Faculty Eng. Appl. Sci., Memorial Univ. Newfoundland, St. John's, NL, Canada, 2015.

[12] D. P. Mandic and S. S. L. Goh, *Complex Valued Nonlinear Adaptive Filters: Noncircularity, Widely Linear and Neural Models* (Adaptive and Learning Systems for Signal Processing, Communications, and Control). Chichester, West Sussex: Wiley, 2009.

[13] T. Gautama, D. P. Mandic, and M. M. Van Hulle, "Signal nonlinearity in fMRI: A comparison between BOLD and MION," *IEEE Trans. Med. Imag.*, vol. 22, no. 5, pp. 636–644, May 2003. [Online]. Available: http://dx.doi.org/10.1109/TMI.2003.812248

[14] T. Gautama, D. P. Mandic, and M. M. Van Hulle, "The delay vector variance method for detecting determinism and nonlinearity in time series," *Phys. D, Nonlinear Phenomena*, vol. 190, nos. 3–4, pp. 167–176, 2004. [Online]. Available: http://dx.doi.org/10.1016/j.physd.2003.11.001

[15] R. G. Andrzejak, K. Lehnertz, F. Mormann, C. Rieke, P. David, and C. E. Elger, "Indications of nonlinear deterministic and finite-dimensional structures in time series of brain electrical activity: Dependence on recording region and brain state," *Phys. Rev. E-Statist., Nonlinear, Soft Matter Phys.*, vol. 64, no. 6I, pp. 061907-1–061907-8, 2001. [Online]. Available: http://dx.doi.org/10.1103/PhysRevE.64.061907

[16] T. Schreiber and A. Schmitz, "Surrogate time series," *Phys. D, Nonlinear Phenomena*, vol. 142, nos. 3–4, pp. 346–382, 2000. [Online]. Available: http://dx.doi.org/10.1016/S0167-2789(00)00043-9

[17] G. R. Arce, *Nonlinear Signal Processing: A Statistical Approach*. Hoboken, NJ, USA: Wiley, 2004.

[18] K. El-Darymli, P. McGuire, D. Power, and C. Moloney, "Target detection in synthetic aperture radar imagery: A state-of-the-art survey," *J. Appl. Remote Sens.*, vol. 7, no. 1, p. 071598, 2013. [Online]. Available: http://dx.doi.org/10.1117/1.JRS.7.071598

[19] M. Novey, T. Adali, and A. Roy, "Circularity and Gaussianity detection using the complex generalized Gaussian distribution," *IEEE Signal Process. Lett.*, vol. 16, no. 11, pp. 993–996, Nov. 2009. [Online]. Available: http://dx.doi.org/10.1109/LSP.2009.2028412

[20] M. J. Wainwright, E. P. Simoncelli, and A. S. Willsky, "Random cascades on wavelet trees and their use in analyzing and modeling natural images," *Appl. Comput. Harmon. Anal.*, vol. 11, no. 1, pp. 89–123, 2001. [Online]. Available: http://dx.doi.org/10.1006/acha.2000.0350

[21] J. G. Proakis, *Digital Signal Processing: Principles, Algorithms, and Applications*, 4th ed. Upper Saddle River, NJ, USA: Prentice-Hall, 2006.

[22] A. V. Oppenheim, R. W. Schafer, M. T. Yoder, and W. T. Padgett, *Discrete-Time Signal Processing*, 3rd ed. Upper Saddle River, NJ, USA: Prentice-Hall, 2009.

[23] J.-P. Antoine, R. Murenzi, P. Vandergheynst, and S. T. Ali, *Two-Dimensional Wavelets and Their Relatives*. Cambridge, U.K.: Cambridge Univ. Press, 2004.

[24] A. D. Poularikas, Ed., *Transforms and Applications Handbook*. Boca Raton, FL, USA: CRC Press, 2010.

[25] R. O. Duda, P. E. Hart, and D. G. Stork, *Pattern Classification*. New York, NY, USA: Wiley, 2001.

[26] N. E. Huang *et al.*, "The empirical mode decomposition and the Hilbert spectrum for nonlinear and non-stationary time series analysis," *Roy. Soc. London Ser. A, Math., Phys. Eng. Sci.*, vol. 454, no. 1971, pp. 903–995, 1998. [Online]. Available: http://dx.doi.org/10.1098/rspa.1998.0193

[27] A. Singer and R. R. Coifman, "Non-linear independent component analysis with diffusion maps," *Appl. Comput. Harmon. Anal.*, vol. 25, no. 2, pp. 226–239, 2008. [Online]. Available: http://dx.doi.org/10.1016/j.acha.2007.11.001

[28] K. El-Darymli, P. McGuire, E. Gill, D. Power, and C. Moloney, "Understanding the significance of radiometric calibration for synthetic aperture radar imagery," in *Proc. IEEE 27th Can. Conf. Elect. Comput. Eng. (CCECE)*, Toronto, ON, Canada, May 2014, pp. 1–6. [Online]. Available: http://dx.doi.org/10.1109/CCECE.2014.6901104

[29] T. G. Leighton, P. R. White, and D. C. Finfer, "Contrast enhancement between linear and nonlinear scatterers," U.S. Patent 20 100 286 514, A1, Nov. 11, 2010. [Online]. Available: http://www.google.ca/patents/US20100286514

[30] T. G. Leighton, G. H. Chua, and P. R. White, "Do dolphins benefit from nonlinear mathematics when processing their sonar returns?" *Roy. Soc. A, Math., Phys. Eng. Sci.*, vol. 468, no. 2147, pp. 3517–3532, 2012. [Online]. Available: http://dx.doi.org/10.1098/rspa.2012.0247

[31] T. G. Leighton, G. H. Chua, P. R. White, K. F. Tong, H. D. Griffiths, and D. J. Daniels, "Radar clutter suppression and target discrimination using twin inverted pulses," *Roy. Soc. A, Math., Phys. Eng. Sci.*, vol. 469, no. 2160, pp. 1–14, 2013. [Online]. Available: http://dx.doi.org/10.1098/rspa.2013.0512

[32] V. Illingworth, Ed., *The Penguin Dictionary of Physics*. London, U.K.: Penguin, 1991.

[33] J. A. Rice, *Mathematical Statistics and Data Analysis*. Belmont, CA, USA: Duxbury Press, 1995.

[34] R. J. Brown and B. Rimmer, *Generalized Central Limit Theorem*. Wolfram Demonstration Project, 2014. [Online]. Available: http://demonstrations.wolfram.com/GeneralizedCentralLimitTheorem/

[35] T. Schreiber and A. Schmitz, "Improved surrogate data for nonlinearity tests," *Phys. Rev. Lett.*, vol. 77, no. 4, pp. 635–638, 1996. [Online]. Available: http://dx.doi.org/10.1103/PhysRevLett.77.635

[36] D. N. Politis, "The impact of bootstrap methods on time series analysis," *Statist. Sci.*, vol. 18, no. 2, pp. 219–230, 2003. [Online]. Available: http://dx.doi.org/10.1214/ss/1063994977

[37] D. Kugiumtzis, I. Vlachos, A. Papana, and P. G. Larsson, "Assessment of measures of scalar time series analysis in discriminating preictal states," *Int. J. Bioelectromagn.*, vol. 9, no. 3, pp. 134–145, 2007. [Online]. Available: http://www.ijbem.org/volume9/number3/090303.pdf

[38] J. Theiler, S. Eubank, A. Longtin, B. Galdrikian, and J. D. Farmer, "Testing for nonlinearity in time series: The method of surrogate data," *Phys. D, Nonlinear Phenomena*, vol. 58, nos. 1–4, pp. 77–94, 1992. [Online]. Available: http://dx.doi.org/10.1016/0167-2789(92)90102-S

[39] D. S. Wilks, *Statistical Methods in the Atmospheric Sciences*, vol. 100, 3rd ed. Waltham, MA, USA: Academic, 2011.

[40] D. Kugiumtzis, "Evaluation of surrogate and bootstrap tests for nonlinearity in time series," *Studies Nonlinear Dyn. Econ.*, vol. 12, no. 1, pp. 1–24, 2008. [Online]. Available: http://dx.doi.org/10.2202/1558-3708.1474

[41] D. Kugiumtzis, "Statically transformed autoregressive process and surrogate data test for nonlinearity," *Phys. Rev. E, Statist., Nonlinear, Soft Matter Phys.*, vol. 66, no. 2, p. 025201, 2002. [Online]. Available: http://dx.doi.org/10.1103/PhysRevE.66.025201

[42] H. G. Schuster and W. Just, *Deterministic Chaos. An Introduction*. Weinheim, Germany: Wiley, 2006.

[43] A. M. Fraser and H. L. Swinney, "Independent coordinates for strange attractors from mutual information," *Phys. Rev. A, Atomic, Molecular, Opt. Phys.*, vol. 33, no. 2, pp. 1134–1140, 1986. [Online]. Available: http://dx.doi.org/10.1103/PhysRevA.33.1134

[44] C. J. Cellucci, A. M. Albano, and P. E. Rapp, "Statistical validation of mutual information calculations: Comparison of alternative numerical algorithms," *Phys. Rev. E, Statist., Nonlinear, Soft Matter Phys.*, vol. 71, no. 6, p. 066208, 2005. [Online]. Available: http://dx.doi.org/10.1103/PhysRevE.71.066208

[45] M. Palus and D. Hoyer, "Detecting nonlinearity and phase synchronization with surrogate data," *IEEE Eng. Med. Biol. Mag.*, vol. 17, no. 6, pp. 40–45, Nov./Dec. 1998. [Online]. Available: http://dx.doi.org/10.1109/51.731319

[46] K. Shi, X. Ma, and G. T. Zhou, "A mutual information based double-talk detector for nonlinear systems," in *Proc. 42nd IEEE Annu. Conf. Inf. Sci. Syst. (CISS)*, Mar. 2008, pp. 356–360. [Online]. Available: http://dx.doi.org/10.1109/CISS.2008.4558551

[47] D. R. Ucci, W. Jacklin, and J. Grimm, "Investigation and simulation of nonlinear processors for spread spectrum receivers," Rome Lab., Air Force Materiel Command, New York, NY, USA, Tech. Rep. RL-TR-93-258, 1993. [Online]. Available: http://www.dtic.mil/cgi-bin/GetTRDoc?Location=U2&doc=GetTRDoc.pdf&AD=ADA278025

[48] M. Paluš, "Testing for nonlinearity using redundancies: Quantitative and qualitative aspects," *Phys. D, Nonlinear Phenomena*, vol. 80, nos. 1–2, pp. 186–205, Jan. 1995. [Online]. Available: http://dx.doi.org/10.1016/0167-2789(95)90079-9

[49] D. S. Moore, G. P. McCabe, and B. A. Craig, *Introduction to the Practice of Statistics*, 6th ed. New York, NY, USA: Freeman, 2009.

[50] M. Abramowitz and I. A. Stegun, *Handbook of Mathematical Functions: With Formulas, Graphs, and Mathematical Tables* (Applied Mathematics), vol. 55. Washington, DC, USA: NBS, 1972.

[51] F. J. Massey, Jr., "The Kolmogorov–Smirnov test for goodness of fit," *J. Amer. Statist. Assoc.*, vol. 46, no. 253, pp. 68–78, Mar. 1951. [Online]. Available: http://www.jstor.org/stable/2280095

[52] G. Marsaglia, W. W. Tsang, and J. Wang, "Evaluating Kolmogorov's distribution," *J. Statist. Softw.*, vol. 8, no. 18, pp. 1–4, 2003. [Online]. Available: http://www.jstatsoft.org/v08/i18

[53] M. A. Stephens, "EDF statistics for goodness of fit and some comparisons," *J. Amer. Statist. Assoc.*, vol. 69, no. 347, pp. 730–737, 1974. [Online]. Available: http://dx.doi.org/10.1080/01621459.1974.10480196

[54] P. J. Schreier and L. L. Scharf, *Statistical Signal Processing of Complex-Valued Data: The Theory of Improper and Noncircular Signals*. Cambridge, U.K.: Cambridge Univ. Press, 2010.

[55] European Southern Observatory. (2015). *Artist's Impression of the Evolution of a Hot High-Mass Binary Star (Annotated Version)*. [Online]. Available: http://www.eso.org/public/videos/eso1230b

[56] J. G. Davis, Jr., "The pronunciations, derivations, and meanings of a selected list of star names," *Popular Astron.*, vol. 52, no. 3, pp. 1–8, 1944. [Online]. Available: http://tinyurl.com/mhr444u

[57] Wikipedia. (2015). *Naval Station Argentia*. [Online]. Available: http://en.wikipedia.org/wiki/Naval_Station_Argentia

[58] MacDonald, Dettwiler and Associates Ltd. (2015). *Radarsat-2 Product Description*. [Online]. Available: http://gs.mdacorporation.com/products/sensor/radarsat2/RS2_Product_Description.pdf

[59] MacDonald, Dettwiler and Associates Ltd. (2015). *Radarsat-2 Sample Dataset*. [Online]. Available: http://gs.mdacorporation.com/SatelliteData/Radarsat2/SampleDataset.aspx

[60] United States Air Force. (2015). *MSTAR*. [Online]. Available: https://www.sdms.afrl.af.mil/index.php?collection=mstar

[61] G. L. Charvat. (2015). *Low-Power X-Band Rail SAR*. [Online]. Available: http://www.glcharvat.com/ Dr. Gregory_L.Charvat_Projects/Low-Power_X-Band_Rail_SAR.html

[62] G. L. Charvat, L. Kempell, and C. Coleman, "A low-power high-sensitivity X-band rail SAR imaging system," *IEEE Antennas Propag. Mag.*, vol. 50, no. 3, pp. 108–115, Jun. 2008. [Online]. Available: http://dx.doi.org/10.1109/MAP.2008.4563576

[63] M. Novey, T. Adali, and A. Roy, "A complex generalized Gaussian distribution—Characterization, generation, and estimation," *IEEE Trans. Signal Process.*, vol. 58, no. 3, pp. 1427–1433, Mar. 2010. [Online]. Available: http://dx.doi.org/10.1109/TSP.2009.2036049

[64] Matlab, *Normal Distribution*. Mathworks R2014b Documentation, 2015. [Online]. Available: http://www.mathworks.com/help/stats/normal-distribution.html

[65] K. El-Darymli, P. McGuire, E. Gill, D. Power, and C. Moloney, "Effect of detection on spatial resolution in synthetic aperture radar imagery and mitigation through upsampling," *J. Appl. Remote Sens.*, vol. 8, no. 1, p. 083601, Jul. 2014. [Online]. Available: http://dx.doi.org/10.1117/1.JRS.8.083601

[66] K. El-Darymli, P. McGuire, E. Gill, D. Power, and C. Moloney, "Holism for target classification in synthetic aperture radar imagery," *IEEE Trans. Aerosp. Electron. Syst.*, to be published.

[67] K. P. Burnham and D. R. Anderson, *Model Selection and Multimodel Inference: A Practical Information-Theoretic Approach*. New York, NY, USA: Springer-Verlag, 2010.

[68] C. D. Manning and H. Schütze, *Foundations of Statistical Natural Language Processing*. Cambridge, MA, USA: MIT Press, 1999.

[69] D. M. Endres and J. E. Schindelin, "A new metric for probability distributions," *IEEE Trans. Inf. Theory*, vol. 49, no. 7, pp. 1858–1860, Jul. 2003. [Online]. Available: http://dx.doi.org/10.1109/TIT.2003.813506

KHALID EL-DARYMLI (M'08) received the B.Sc. degree in electrical engineering from the Garyounis University of Libya, the M.Sc. degree in computer and information engineering from International Islamic University Malaysia, and the Ph.D. degree in electrical engineering Passed with Distinction from the Memorial University of Newfoundland, Canada. He is currently a Senior Engineer with Northern Radar Inc. His special research interests include holism, nonlinear/dispersive scattering, adaptive, nonlinear and chaos theory inspired methods for signal processing, and target recognition in radar imagery. He is a member of the Association of Professional Engineers and Geoscientists of Alberta, and a fellow of the School of Graduate Studies, Memorial University of Newfoundland.

ERIC W. GILL (M'00–SM'05) received the B.Sc. (Hons.) degree in physics and the M.Eng. and Ph.D. degrees in electrical engineering from the Memorial University of Newfoundland (MUN), St. John's, NL, Canada, in 1977, 1990, and 1999, respectively. For over two decades, starting in 1977, he was a Lecturer in Physics and Mathematics with the provincial college system, and for a significant period during those years, he pursued research interests in rough surface electromagnetic scattering theory. He is currently a Professor with the Department of Electrical and Computer Engineering, MUN, where he teaches and conducts research on theoretical and applied electromagnetics. His special interest lies in the scattering of high-frequency electromagnetic radiation from time varying, and randomly rough surfaces, with a particular application to the use of high-frequency surface wave radar in remote sensing of the marine environment. His latest pursuits include ocean remote sensing using both *X*-band nautical radar and synthetic aperture radar. He is a member of the American Geophysical Union.

PETER MCGUIRE received the B.A.Sc. (Eng.) and Ph.D. degrees in aerospace engineering from the University of Toronto. He studied the use of artificial neural networks for computer vision and control of dynamic systems with the University of Toronto. Since joining C-CORE, he has specialized in image processing, earth observation, and data fusion projects. His projects include earth observation using a virtual synthetic aperture radar (SAR) constellation of satellites, sensor management, and data fusion system design using holonic control, along with high-speed automated inspection using computer vision. In addition to project-related activities, he is cross-appointed with the Memorial University of Newfoundland, where he manages a research program focused on oil- and gas-related issues. His topics include detection and mapping of oil under ice using autonomous underwater vehicles, advanced techniques for monitoring targets and infrastructure using satellite and ground-based SAR, coordination of aerial and ground-based robotic systems, and sense and avoid algorithms for unmanned aerial vehicles.

DESMOND POWER (M'11) received the M.Eng. and B.Eng. degrees. He started his career in terrestrial radar, working as an RF Designer in over-the-horizon radar. He was involved in signal processing and analysis of radar data. After the launch of RADARSAT in 1995, he moved into projects related to earth observation, with his first project dealing with iceberg detection capabilities of synthetic aperture radar. Since that time, he has managed and been a Technical Advisor to a large series of projects with C-CORE involving earth observation, including marine target detection, vehicle detection along right-of-ways, and interferometry for ground deformation measurement. He has over 24 years of experience in radar and remote sensing. He is currently the Vice President of Remote Sensing with C-CORE. He is actively involved in the development of terrestrial-based radar systems. He is a Principal Investigator of the multimillion-dollar research and development project on radar-based critical infrastructure monitoring funded by the Atlantic Innovation Fund. He is a member of the Association of Professional Engineers and Geoscientists of Newfoundland and Labrador.

CECILIA MOLONEY (M'91) received the B.Sc. (Hons.) degree in mathematics from the Memorial University of Newfoundland, Canada, and the M.A.Sc. and Ph.D. degrees in systems design engineering from the University of Waterloo, Canada. From 2004 to 2009, she held the NSERC/Petro-Canada Chair for Women in Science and Engineering, Atlantic Region. Since 1990, she has been a Faculty Member with the Memorial University of Newfoundland, where she is currently a Full Professor of Electrical and Computer Engineering. Her research interests include nonlinear signal and image processing methods, signal representations via wavelet and contourlet transforms, radar signal processing, transformative pedagogy for science and engineering, and gender and science studies.

● ● ●